

Multi-Grid Monte Carlo

III. Two-Dimensional $O(4)$ -Symmetric Nonlinear σ -Model

Robert G. Edwards
Supercomputer Computations Research Institute
Florida State University
Tallahassee, FL 32306 USA
Internet: EDWARDS@MAILER.SCRI.FSU.EDU

Sabino José Ferreira*
Department of Physics
New York University
4 Washington Place
New York, NY 10003 USA
Internet: FERREIRA@MAFALDA.PHYSICS.NYU.EDU

Jonathan Goodman[†]
Courant Institute of Mathematical Sciences
New York University
251 Mercer St.
New York, NY 10012 USA
Internet: GOODMAN@NYU.EDU

Alan D. Sokal
Department of Physics
New York University
4 Washington Place
New York, NY 10003 USA
Internet: SOKAL@ACF3.NYU.EDU

August 27, 2018

*Address after September 1, 1991: Departamento de Física – ICEx, Universidade Federal de Minas Gerais, Caixa Postal 702, Belo Horizonte MG 30161, BRAZIL. Bitnet: SABINO@BRUFMG.BITNET

[†]Address from September 1, 1991 to June 30, 1992: Department of Mathematics, Stanford University, Stanford CA 94305, USA. Internet: GOODMAN@CAUCHY.STANFORD.EDU

Abstract

We study the dynamic critical behavior of the multi-grid Monte Carlo (MGMC) algorithm with piecewise-constant interpolation applied to the two-dimensional $O(4)$ -symmetric nonlinear σ -model [= $SU(2)$ principal chiral model], on lattices up to 256×256 . We find a dynamic critical exponent $z_{int, \mathcal{M}^2} = 0.60 \pm 0.07$ for the W-cycle and $z_{int, \mathcal{M}^2} = 1.13 \pm 0.11$ for the V-cycle, compared to $z_{int, \mathcal{M}^2} = 2.0 \pm 0.15$ for the single-site heat-bath algorithm (subjective 68% confidence intervals). Thus, for this asymptotically free model, critical slowing-down is greatly reduced compared to local algorithms, but not completely eliminated. For a 256×256 lattice, W-cycle MGMC is about 35 times as efficient as a single-site heat-bath algorithm.

1 Introduction

By now it is widely recognized [1, 2, 3, 4] that better simulation algorithms, with strongly reduced critical slowing-down, are needed for high-precision Monte Carlo studies of statistical-mechanical systems near critical points and of quantum field theories (such as QCD) near the continuum limit. One promising class of such algorithms is *multi-grid Monte Carlo* (MGMC) [5, 6, 7]. In paper I of this series [6], we explained the conceptual foundations of the MGMC method, and proved the absence of critical slowing-down for Gaussian (free-field) MGMC. In paper II [7], we applied MGMC to the two-dimensional ferromagnetic XY model, and analyzed the dynamic critical behavior in the high-temperature (vortex) and low-temperature (spin-wave) phases (see also [8]).

In the present paper we apply MGMC to the two-dimensional $O(N)$ -symmetric nonlinear σ -model (also called N -vector model) with $N = 4$, defined by

$$H(\boldsymbol{\sigma}) = -\beta_{O(4)} \sum_{\langle xx' \rangle} \boldsymbol{\sigma}_x \cdot \boldsymbol{\sigma}_{x'} , \quad (1.1)$$

where each spin $\boldsymbol{\sigma}_x$ is a unit vector in \mathbb{R}^4 , $\langle xx' \rangle$ runs over all nearest-neighbor pairs, and $\beta_{O(4)} > 0$ is the inverse temperature in the $O(4)$ normalization. Since the sphere S^3 is isometric (as a Riemannian manifold) to the group $SU(2)$ via the map

$$g = \begin{pmatrix} \sigma^0 + i\sigma^3 & \sigma^2 + i\sigma^1 \\ -\sigma^2 + i\sigma^1 & \sigma^0 - i\sigma^3 \end{pmatrix} , \quad (1.2)$$

this model can also be thought of as the $SU(2)$ principal chiral model

$$H(g) = -\beta_{SU(2)} \sum_{\langle xx' \rangle} \text{Re tr}(g_x^\dagger g_{x'}) , \quad (1.3)$$

with $\beta_{SU(2)} = \beta_{O(4)}/2$. Our principal aim is to make a careful study of the dynamic critical behavior of the MGMC algorithm for this asymptotically free model, and in particular to extract the dynamic critical exponent(s). We also take advantage of the high efficiency of the MGMC algorithm — about 35 times that of a single-site heat-bath algorithm, on a 256×256 lattice — to make a detailed comparison of the static scaling behavior with the asymptotic-freedom predictions.

Two-dimensional N -vector models are of direct interest in condensed-matter physics, and they are important “toy models” in elementary-particle physics by virtue of their close similarity to four-dimensional gauge theories. They have therefore been extensively studied by rigorous [9, 10, 11, 12, 13], exact-but-nonrigorous [14, 15, 16, 17, 18, 19], renormalization-group [20, 21, 22, 23, 24, 25, 26, 27, 28, 29], high-temperature expansion [30, 31, 32], $1/N$ expansion [33, 34, 35, 36, 37, 38] and Monte Carlo [39, 40, 41, 42, 43, 44, 45, 46, 47, 48, 49] methods.¹ It is known rigorously that every infinite-volume Gibbs measure is invariant under global spin rotations [11] and in particular has zero spontaneous magnetization [9]; it

¹ This is a *very* incomplete set of references, but a significant fraction of the relevant articles can be tracked down starting from these. Also, studies dealing solely with the XY case are cited in [7] and therefore omitted here.

is believed, though not yet proven, that at each β there is a *unique* infinite-volume Gibbs measure.²

Renormalization-group calculations in the low-temperature expansion (\equiv weak-coupling perturbation theory) [20, 21] suggest that the N -vector models with $N > 2$ are *asymptotically free* — i.e. that the only critical point is at $\beta = \infty$ — and that the correlation length ξ and susceptibility χ behave as

$$\xi(\beta) = C_\xi \beta^{-1/(N-2)} e^{2\pi\beta/(N-2)} \left[1 + \frac{a_1}{\beta} + \frac{a_2}{\beta^2} + \dots \right] \quad (1.4)$$

$$\chi(\beta) = C_\chi \beta^{-(N+1)/(N-2)} e^{4\pi\beta/(N-2)} \left[1 + \frac{b_1}{\beta} + \frac{b_2}{\beta^2} + \dots \right] \quad (1.5)$$

as $\beta \rightarrow \infty$.³ Here the a_k and b_k are nonuniversal constants (depending on N) that can be computed in weak-coupling perturbation theory on the lattice at $k + 2$ loops; in particular, a_1 and b_1 have been computed for the nearest-neighbor action (1.1) and two variant actions [26, 29].⁴ On the other hand, C_ξ and C_χ are nonuniversal constants (depending on N) that have to be computed by some non-perturbative method. For the exponential correlation length (= inverse mass gap), the coefficient $C_\xi \equiv 2^{-5/2} [(N-2)/(2\pi e^{\pi/2})]^{1/(N-2)} (m/\Lambda_{\overline{\text{MS}}})^{-1}$ has⁵ been computed exactly using the Bethe Ansatz [17, 18, 19]: the result is

$$\frac{m}{\Lambda_{\overline{\text{MS}}}} = \left(\frac{8}{e}\right)^{1/(N-2)} \frac{1}{\Gamma\left(1 + \frac{1}{N-2}\right)}. \quad (1.6)$$

The asymptotic-freedom predictions (1.4)/(1.5) have not yet been proven rigorously (but see [50, 51, 52, 53] for some progress), and indeed they have been questioned by one group [54, 55, 56]. However, they are consistent with Monte Carlo studies for $N = 3$ [44, 45, 48], $N = 4$ [40, 42, 46] and $N = 8$ [46]. More precisely, for $N = 3$ it is found that for $1.5 \lesssim \beta \lesssim 2.05$ (corresponding to $10 \lesssim \xi \lesssim 300$), the quantity C_ξ defined by (1.4) varies by about 20% — contrary to the prediction that it should be constant — and also differs by about 20% from the predicted exact value (1.6). It appears, therefore, that *quantitative* asymptotic scaling has not yet set in at $\xi \sim 100$, even though the qualitative behavior is correct. For

² In the XY case it has been proven that there is a unique *translation-invariant* infinite-volume Gibbs measure [12, 13].

³ In this paper the susceptibility is defined as $\chi = \sum_x \langle \sigma_0 \cdot \sigma_x \rangle$. This definition is employed also in [26, 30, 33, 35, 36, 40, 42]. By contrast, the standard thermodynamic definition is $\chi_{thermo} = \beta \chi_{this\ paper}$; the extra factor of β arises because the inverse temperature β is introduced as an overall factor multiplying also the magnetic field. The thermodynamic definition is employed in [21, 28]. This difference in notation must be borne in mind when comparing results in the literature!

⁴ Reference [26] employs, as we do, the *second-moment* definition of the correlation length: compare equation (12a) of [26] with (3.14)/(3.17) below. Several other papers (e.g. [44, 45, 48, 17, 18, 19, 46]) emphasize, by contrast, the *exponential* correlation length (= inverse mass gap). The coefficients a_1, a_2, \dots and C_ξ need not be the same for the two quantities.

⁵ This relation between C_ξ and $m/\Lambda_{\overline{\text{MS}}}$ is based on the result $\Lambda_{\overline{\text{MS}}}/\Lambda_{lat} = 2^{5/2} e^{\pi/2(N-2)}$ from lattice perturbation theory [23, 24]. Please note that equation (3) of [46] suffers from a typographical error: the division sign should be multiplication.

$N = 4, 8$, however, the agreement with (1.4) is better; this suggests that as N increases, asymptotic scaling sets in at smaller values of ξ [46].

A very similar picture has been obtained by Padé extrapolation of high-temperature series [30, 31, 32]. It is found that the critical singularity in the complex β -plane, which lies at real β when $-2 \leq N \leq 2$, bifurcates for $N > 2$ into a pair of complex-conjugate singularities, which tend as $N \rightarrow \infty$ to $\tilde{\beta} \equiv \beta/N \approx 0.32162(1 \pm i)$. In particular, for $N = 3$, this first pair of singularities is located at $\beta \approx 1.73 \pm 0.42i$ [32, Figure 2], extremely close to the real axis and to the region in which the Monte Carlo simulations are currently being performed ($\beta = 1.73$ corresponds to $\xi \approx 42$). By contrast, for $N = 4$ the first singularity has moved to $\beta \approx 2.27 \pm 0.88i$, i.e. farther away from the real axis and also towards smaller ξ ($\beta = 2.27$ corresponds to $\xi \approx 17$). For $N = 8$ the first singularity is located at $\beta \approx 3.78 \pm 2.38i$ ($\beta = 3.78$ corresponds to $\xi \approx 5$).⁶ It is thus very plausible that these complex singularities are responsible for preventing asymptotic scaling for $\xi \sim 100$ at $N = 3$.

Let us remark that by eliminating β from (1.4)/(1.5), we obtain

$$\chi = C_{\chi\xi} \xi^2 (\log \xi)^{-(N-1)/(N-2)} \left[1 + c_{11} \frac{\log \log \xi}{\log \xi} + c_{01} \frac{1}{\log \xi} + O\left(\frac{\log^2 \log \xi}{\log^2 \xi}\right) \right], \quad (1.7)$$

where

$$c_{11} = -\frac{N-1}{(N-2)^2} \quad (1.8a)$$

$$c_{01} = \frac{N-1}{(N-2)^2} \left[\log \frac{2\pi}{N-2} + (N-2) \log C_\xi \right] + \frac{2\pi}{N-2} (b_1 - 2a_1) \quad (1.8b)$$

In finite volume (with periodic boundary conditions), the usual finite-size-scaling Ansatz gives, up to corrections of order β^{-1} ,

$$\xi(\beta, L) = \beta^{-1/(N-2)} e^{2\pi\beta/(N-2)} f_\xi(\xi_\infty/L) \quad (1.9)$$

$$\chi(\beta, L) = \beta^{-(N+1)/(N-2)} e^{4\pi\beta/(N-2)} f_\chi(\xi_\infty/L) \quad (1.10)$$

where f_ξ and f_χ are finite-size-scaling functions, and $\xi_\infty \equiv \xi(\beta, \infty)$. Note that $\lim_{x \rightarrow 0} f_\xi(x) = C_\xi > 0$ and likewise for f_χ . One can also eliminate β from (1.9)/(1.10), yielding

$$\chi(\beta, L) = \xi(\beta, L)^2 [\log \xi(\beta, L)]^{-(N-1)/(N-2)} f_{\chi\xi}(\xi_\infty/L) \quad (1.11)$$

up to corrections of order $\log \log \xi / \log \xi$. The Ansätze (1.9)–(1.11) can be written in numerous equivalent forms, for example,

$$\xi(\beta, L) = \beta^{-1/(N-2)} e^{2\pi\beta/(N-2)} \tilde{f}_\xi(\xi/L) \quad (1.12)$$

$$\chi(\beta, L) = \beta^{-(N+1)/(N-2)} e^{4\pi\beta/(N-2)} \tilde{f}_\chi(\xi/L) \quad (1.13)$$

$$\chi(\beta, L) = \xi^2 (\log \xi)^{-(N-1)/(N-2)} \tilde{f}_{\chi\xi}(\xi/L) \quad (1.14)$$

where $\xi \equiv \xi(\beta, L)$.

⁶ We thank Paolo Butera for providing us with precise numerical values of the singularity locations first reported in [32, Figure 2].

2 MGMC Algorithm for Nonlinear σ -Models

The physical causes of critical slowing-down in the traditional (local) Monte Carlo algorithms, and the motivation for collective-mode algorithms, have been discussed previously [1, 6, 4]. In particular, paper I [6] provides an extensive treatment of the physics behind MGMC and the details of its implementation, as well as a comparison with other types of collective-mode algorithms (Fourier acceleration and auxiliary-variable algorithms). Here we confine ourselves to a brief review of the structure of the MGMC algorithm as applied to a nonlinear σ -model. We begin by considering a principal chiral model, i.e. a σ -model taking values in some *group* $G \subset U(N)$. At the end of this section we shall make some brief remarks about the more general case of a σ -model taking values in a homogeneous space $M = G/H$.

Consider a principal chiral model with values in $G \subset U(N)$, defined on a d -dimensional lattice of linear size L ; for simplicity let us use a hypercubic lattice with periodic boundary conditions. The Hamiltonian is given by

$$H(g) = -\beta \sum_{\langle xx' \rangle} \text{Re tr}(g_x^\dagger g_{x'}) , \quad (2.1)$$

and the Gibbs probability distribution is

$$d\mu(g) = Z^{-1} \exp[-H(g)] \prod_x dg_x , \quad (2.2)$$

where dg is Haar measure on G . Our goal is to devise a stochastic updating procedure that leaves invariant the probability distribution (2.2) and has an autocorrelation time τ which is as small as possible.

The MGMC algorithm for this model is defined as follows [6, Sections IV and VII]: We first introduce, in addition to the original lattice Ω , a sequence of *coarse grids* $\Omega_M \equiv \Omega, \Omega_{M-1}, \Omega_{M-2}, \dots, \Omega_0$ of linear size $L, L/2, L/4, \dots, L/2^M$, respectively.⁷ These coarse grids will play a role in intermediate stages of the multi-grid algorithm. Each site y of a grid Ω_{l-1} is considered to be associated with a 2^d block B_y in the next-finer grid Ω_l (Figure 1). We define, therefore, an *interpolation operator* $p_{l,l-1}$ that maps a field configuration $g^{(l-1)}$ on grid Ω_{l-1} into one on grid Ω_l , using *piecewise-constant interpolation*:⁸

$$(p_{l,l-1}g^{(l-1)})_x = g_y^{(l-1)} \quad \text{for } x \in B_y . \quad (2.3)$$

Each coarse-grid field is to be thought of as a *correction* or *update* to the next-finer-grid field, acting by left multiplication: that is, given a “fine-grid” field $g^{(l,old)}$ and a “coarse-grid” field $g^{(l-1)}$, we define an updated “fine-grid” field $g^{(l,new)} \equiv (p_{l,l-1}g^{(l-1)})g^{(l,old)}$, or in detail

$$g_x^{(l,new)} = g_y^{(l-1)} g_x^{(l,old)} \quad \text{for } x \in B_y . \quad (2.4)$$

On each grid Ω_l , we consider Hamiltonians H_l of the form

$$H_l(g) = - \sum_{\langle xx' \rangle} \text{Re tr}(\alpha_{xx'}^{(l)} g_x^\dagger g_{x'}) , \quad (2.5)$$

⁷ Clearly L must be a multiple of 2^M . It is therefore most convenient for L to be a power of 2, or at least a power of 2 times a small integer.

⁸ This update had been proposed earlier, in a “unigrid” context, by Meyer-Ortmanns [57].

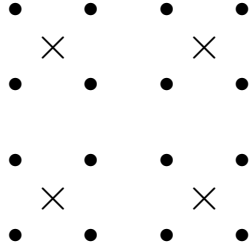


Figure 1: Staggered coarsening (factor-of-2) in dimension $d = 2$. Dots (\bullet) are fine-grid sites, crosses (\times) are coarse-grid sites.

where $\alpha_{xx'}^{(l)}$ is an $N \times N$ complex matrix; note that $\alpha_{xx'}^{(l)}$ is not necessarily unitary or a multiple of a unitary matrix, and it can vary from one bond $\langle xx' \rangle$ to another. On the finest grid ($l = M$) we have $\alpha_{xx'}^{(M)} = \beta I$ for all $\langle xx' \rangle$, but on coarser grids more general Hamiltonians of the form (2.5) will be generated [see (2.7) below].

For each Hamiltonian H_l of the form (2.5), we assume that there is given a *basic stochastic iteration* $g \rightarrow \mathcal{G}_l(g, H_l)$ that updates the field configuration g (which lives on grid Ω_l) in such a way as to leave invariant the probability distribution $\sim \exp[-H_l(g)]$. For concreteness, we shall take \mathcal{G}_l to be the single-site heat-bath algorithm for the Hamiltonian H_l . Finally, we let γ be a positive integer, called the *cycle control parameter*; it will control the number of times that the coarse grids are visited.

The multi-grid Monte Carlo (MGMC) algorithm is then defined recursively as follows:

```

procedure mgmc( $l, g, H_l$ )
comment This algorithm updates a field configuration  $g$  in such a
           way as to leave invariant the Gibbs distribution  $\exp[-H_l(g)] dg$ .

for  $j = 1$  until  $m_1$  do  $g \leftarrow \mathcal{G}_l(g, H_l)$ 
if  $l > 0$  then
    compute  $H_{l-1}(\cdot) \equiv H_l((p_{l,l-1} \cdot)g)$ 
     $h \leftarrow I$ 
    for  $j = 1$  until  $\gamma$  do mgmc( $l - 1, h, H_{l-1}$ )
     $g \leftarrow (p_{l,l-1}h)g$ 
endif
for  $j = 1$  until  $m_2$  do  $g \leftarrow \mathcal{G}_l(g, H_l)$ 
end

```

We see, then, that a single MGMC iteration at level l consists of three steps:

1) *Pre-sweep*. We apply a few (m_1) iterations of the basic stochastic iteration (i.e. single-site heat-bath) at level l . This produces a new field configuration g that differs significantly

from the old one in its short-wavelength components, but not (unfortunately!) in its long-wavelength components.

2) *Coarse-grid correction.* We compute the coarse-grid Hamiltonian $H_{l-1}(h) \equiv H_l((p_{l,l-1}h)g)$. As explained earlier, the coarse-grid field h should be thought of as a correction to g . We initialize the coarse-grid-correction field h to the identity matrix, and make γ updates of this field using MGMC itself (at level $l-1$). We then transfer the updated field h back to grid Ω_l using the interpolation operator $p_{l,l-1}$, and use it to correct the field g . The goal of this coarse-grid correction step is to update rapidly the long-wavelength components of g .

3) *Post-sweep.* We apply, for good measure, a few (m_2) more iterations of the basic stochastic iteration at level l .

Let us now look more closely at some aspects of the MGMC algorithm:

Recursive definition. We have defined the MGMC algorithm recursively — in the coarse-grid correction step the procedure *mgmc* calls itself — because that is by far the simplest and clearest approach. However, the MGMC algorithm can be implemented in *any* computer programming language, including those (like Fortran) that forbid recursive subroutine calls, although the control structure may be a bit more complicated. See [58, Section 4.1] for Fortran and Algol implementations of the multi-grid control structure. Our codes are available on request (preferably via electronic mail).

Computation of H_{l-1} . Assume that the Hamiltonian H_l on level l is of the form (2.5). Then a simple computation shows that the coarse-grid Hamiltonian $H_{l-1}(h) \equiv H_l((p_{l,l-1}h)g)$ is⁹

$$H_{l-1}(h) = - \sum_{\langle yy' \rangle} \text{Re tr}(\alpha_{yy'}^{(l-1)} h_y^\dagger h_{y'}) + \text{const} , \quad (2.6)$$

where

$$\alpha_{yy'}^{(l-1)} = \sum_{\substack{\langle xx' \rangle \\ x \in B_y \\ x' \in B_{y'}}} g_{x'} \alpha_{xx'}^{(l)} g_x^\dagger . \quad (2.7)$$

Note that the coarse-grid Hamiltonian H_{l-1} has the same functional form as the “fine-grid” Hamiltonian H_l : it is specified by the coefficients $\{\alpha_{yy'}^{(l-1)}\}$. The step “*compute H_{l-1}* ” therefore means to compute these coefficients. Note also the importance of generalizing the Hamiltonian from (2.1) to (2.5): even if the fine-grid coefficients are $\alpha_{xx'}^{(M)} = \beta I$ with $\beta > 0$ independent of $\langle xx' \rangle$, the coarse-grid coefficients $\alpha_{xx'}^{(l)}$ for $l < M$, defined by (2.7), will be β times arbitrary finite sums of elements of G , considered in the space \mathbf{M}_N of all complex $N \times N$ matrices. For $G = SU(N)$ with $N \geq 3$, the finite sums of G are dense in \mathbf{M}_N . The group $G = SU(2)$ is a special case: every linear combination of $SU(2)$ matrices (with real

⁹ Note that equation (4.9) of [6] contains a slight error: the sum should be restricted to *nearest-neighbor* pairs $\langle xx' \rangle$ satisfying $x \in B_y$, $x' \in B_{y'}$. A more serious error in [6] arises from our attempt to allow there an arbitrary compact but *not-necessarily-unitary* group $G \subset GL(N, \mathbb{C})$. In such a case the nearest-neighbor pairs $\langle xx' \rangle$ with x and x' belonging to the *same* block B_y make a non-constant contribution to the coarse-grid Hamiltonian, of the form $\text{Re tr}(\alpha_{yy}^{(l-1)} h_y^\dagger h_y)$. It is thus necessary to generalize the Hamiltonian (2.5) to include both nearest-neighbor pairs $\langle xx' \rangle$ and “diagonal” terms $x = x'$; such a form is then preserved under coarsening. We thank Tereza Mendes for pointing out these errors.

coefficients) is a nonnegative multiple of an $SU(2)$ matrix, as can be seen from (1.2). Such a matrix can therefore be represented in the form (1.2) but without the constraint $\sigma^2 = 1$.

Note also an important qualitative distinction between the original Hamiltonian (2.1) and the “frustrated” Hamiltonian (2.5)¹⁰: the Hamiltonian (2.1) has a $G \times G$ global symmetry $g_x \rightarrow hg_xh'$, while the Hamiltonian (2.5) has only the G symmetry of *left* multiplication $g_x \rightarrow hg_x$. (If one *right*-multiplies g_x and $g_{x'}$ by an element h' that does not commute with $\alpha_{xx'}^{(l)}$, the energy changes.) Fortunately, it is only the *left* symmetry that is exploited in the passage (2.4) to yet coarser grids. (The coarse-grid-correction move should be a symmetry *within* each block, and contribute an energy only *between* blocks.) Of course, this fortunate circumstance is not a coincidence: from the “unigrid” interpretation [60, 6] one sees that left-multiplication on a very coarse grid acts simply as left-multiplication on a very large block on the fine grid — which is of course a symmetry within the block.

It should also be emphasized that the coefficients in the coarse-grid Hamiltonian (2.6) depend implicitly on the current fine-grid field configuration g . Finally, let us emphasize that in the MGMC algorithm, unlike the corresponding deterministic MG algorithm, the coarse-grid Hamiltonian *must* (as far as we can tell) be defined by the “variational formula” $H_{l-1}(h) \equiv H_l((p_{l,l-1}h)g)$; only in this way does the algorithm leave invariant the correct Gibbs distribution (2.2).¹¹

Choice of \mathcal{G}_l . The basic stochastic iteration $\mathcal{G}_l(\cdot, H_l)$ can, in principle, be *any* stochastic updating procedure that leaves invariant the probability distribution $\sim \exp[-H_l(g)]$. It could, for example, be a single-site (possibly multi-hit) Metropolis algorithm, or a single-site quasi-heat-bath [61] algorithm. Indeed, a quasi-heat-bath algorithm may turn out to be the most efficient one in practice (taking into account CPU time). However, for conceptual and experimental purposes, a pure heat-bath algorithm is far preferable, as it is a clearly defined object with no free parameters. By contrast, the effectiveness of a Metropolis (or quasi-heat-bath) algorithm can vary dramatically as a function of the hit size (or underlying Von Neumann proposal algorithm) and the Hamiltonian H_l . This is a particularly severe problem in MGMC, as the coefficients in H_l are *random* and highly variable. We have therefore used a pure heat-bath algorithm (with red-black ordering) in all our experiments. Technical details of this algorithm can be found in Appendix A.

Pre-sweeps vs. post-sweeps. The balance between pre-sweeps and post-sweeps is not very crucial; only the total $m_1 + m_2$ seems to matter much. Indeed, either the pre-sweep or the post-sweep (but not both!) could be eliminated entirely. Increasing m_1 and m_2 improves the performance of the MGMC iteration, at the expense of increased computational labor per iteration. In this paper we have always taken $m_1 = m_2 = 1$, but we make no claim that this is optimal.

Cycle control parameter γ and computational labor. Clearly, one iteration of the multi-grid algorithm at level M comprises one visit to grid M , γ visits to grid $M - 1$, γ^2 visits to

¹⁰ The Hamiltonian (2.5) can also be thought of as a principal chiral model in a fixed background “dielectric gauge field” [59].

¹¹ This point has caused some confusion in the literature; for further discussion and references, see [6, Section X.A].

grid $M - 2$, and so on. Thus, γ determines the degree of emphasis placed on the coarse-grid updates. ($\gamma = 0$ would correspond to the pure heat-bath iteration on the finest grid alone.)

We can now estimate the computational labor required for one iteration of the multi-grid algorithm. Each visit to a given grid involves $m_1 + m_2$ heat-bath sweeps on that grid, plus the work involved in computing the coarse-grid Hamiltonian and in carrying out the interpolation back to the fine-grid. The work involved in all these operations is proportional to the number of lattice points on that grid. Let W_l be the work required for these operations on grid l . Then, for grids defined by a factor-of-2 coarsening in d dimensions, we have

$$W_l \approx 2^{-d(M-l)} W_M, \quad (2.8)$$

so that the total work for one multi-grid iteration is

$$\begin{aligned} \text{work}(MG) &= \sum_{l=M}^0 \gamma^{M-l} W_l \\ &\approx W_M \sum_{l=M}^0 (\gamma 2^{-d})^{M-l} \\ &\leq W_M (1 - \gamma 2^{-d})^{-1} \quad \text{if } \gamma < 2^d. \end{aligned} \quad (2.9)$$

Thus, provided that $\gamma < 2^d$, the work required for one entire multi-grid iteration is no more than $(1 - \gamma 2^{-d})^{-1}$ times the work required for $m_1 + m_2$ heat-bath iterations (plus a little auxiliary computation) on the finest grid alone — *irrespective of the total number of levels*. The most common choices are $\gamma = 1$ (the V-cycle) and $\gamma = 2$ (the W-cycle), but we shall also consider $\gamma = 3$ (the “super-W-cycle” or S-cycle).

MGMC vs. renormalization group. We wish to emphasize that although the multi-grid method and the block-spin renormalization group (RG) are based on very similar *philosophies* — dealing with a single length scale at a time — they are in fact *very different*. In particular, the conditional coarse-grid Hamiltonian H_{l-1} employed in the MGMC method is *not* the same as the renormalized Hamiltonian given by a block-spin RG transformation. The RG transformation computes the *marginal*, not the conditional, distribution of the block means — that is, it *integrates* over the complementary degrees of freedom, while the MGMC method *fixes* these degrees of freedom at their current (random) values. Our conditional Hamiltonian is given by an explicit finite expression, while the marginal (RG) Hamiltonian cannot be computed in closed form. The failure to appreciate these distinctions has led to some confusion in the literature; for discussion, see [6, Section X.A].

Behavior of Gaussian MGMC. An analogous MGMC algorithm can be devised for the Gaussian model (free field)

$$H(\varphi) = \frac{A}{2} \sum_{\langle xx' \rangle} (\varphi_x - \varphi_{x'})^2 + \frac{B}{2} \sum_x \varphi_x^2, \quad (2.10)$$

and its behavior can be predicted analytically. A simple Fock-space argument [5, 6] shows that the autocorrelation time of the Gaussian MGMC algorithm is *equal* to the convergence time of the corresponding deterministic MG algorithm for solving Laplace’s equation. The deterministic MG algorithm is known to behave as follows:

- Critical slowing-down is completely eliminated for $\gamma \geq 1$ (i.e. at least a V-cycle) with piecewise-linear or smoother interpolation [62], and for $\gamma \geq 2$ (i.e. at least a W-cycle) with piecewise-constant interpolation [63].
- For a V-cycle with piecewise-constant interpolation, the exact behavior is not known, but it is strongly suspected [64, section 4.7] and observed in preliminary numerical tests [65, 66] that the critical slowing-down is *not* eliminated, and that the dynamic critical exponent is in fact $z = 1$.

The behavior of Gaussian MGMC will be a useful standard of comparison for the behavior of MGMC in asymptotically free continuous-spin models.

Remark. Parisi [74] and Mack and collaborators [67, 68, 47, 69] have pointed out that an update of amplitude A on a block of linear size ℓ_B costs an energy $\Delta E \sim \ell_B^{d-2} A^2$ if a smooth (i.e. once-continuously-differentiable) kernel is employed, while it costs a much larger energy $\Delta E \sim \ell_B^{d-1} A^2$ in the case of a piecewise-constant kernel. Thus, the typical update amplitude is $A \sim \ell_B^{-(d-2)/2}$ in the case of a smooth kernel — and this is the “correct” amplitude for an excitation on scale $\sim \ell_B$ in the Gaussian model — while the amplitude is only $A \sim \ell_B^{-(d-1)/2}$ in the case of piecewise-constant (step-function) kernel, i.e. a factor $\sqrt{\ell_B}$ “too small”. (This behavior is confirmed numerically [47].) From these facts one might expect that MGMC with piecewise-constant interpolation would *not* succeed in eliminating critical slowing-down for the Gaussian model. However, this conclusion is only partially correct: as explained above, the rigorous analysis [63] shows that piecewise-constant MGMC *does* eliminate critical slowing-down provided that at least a W-cycle is employed ($\gamma \geq 2$). Apparently what is happening is that the multiple updates per iteration — $\ell_B^{\log_2 \gamma}$ of them on length scale ℓ_B — compensate for the unduly small amplitude of each individual update. Unfortunately, we are unable to make this heuristic argument quantitative, because we do not know to what extent these multiple updates are correlated. In particular, we are unable to translate the rigorous proof into a heuristic argument in a way that is quantitatively correct (i.e. yields the correct critical exponent z as a function of γ).

Now let us make a few further remarks:

MGMC for general σ -models. Thus far we have considered the MGMC algorithm for a σ -model taking values in some group $G \subset U(N)$. Now let us consider a σ -model taking values in some manifold M on which a compact group $G \subset U(N)$ acts transitively. Then, by fixing a reference configuration $\bar{\varphi} = \{\bar{\varphi}_x\}_{x \in \Omega} \in M^\Omega$, we can define a (many-to-one) map of G^Ω onto M^Ω by

$$\{g_x\} \longrightarrow \{g_x \bar{\varphi}_x\}. \quad (2.11)$$

In particular, Haar measure on G^Ω is mapped onto Haar measure on M^Ω . Likewise, all observables F on M^Ω — including the Hamiltonian — can be “lifted” to G^Ω :

$$\tilde{F}(g) \equiv F(g\bar{\varphi}). \quad (2.12)$$

Then the expectation value of any observable $F(\varphi)$ with respect to the Hamiltonian $H(\varphi)$ [and Haar measure on M^Ω] is equal to the expectation value of $\tilde{F}(g)$ with respect to the

Hamiltonian $\widetilde{H}(g)$ [and Haar measure on G^Ω]:

$$\int F(\varphi) e^{-H(\varphi)} \prod_x d\varphi_x = \int \widetilde{F}(g) e^{-\widetilde{H}(g)} \prod_x dg_x, \quad (2.13)$$

where $d\varphi_x$ and dg_x are normalized Haar measure on M and G , respectively. Thus, the σ -model taking values in M can be “lifted” to a σ -model taking values in G .

Consider, for example, the N -vector model: here M is the unit sphere in \mathbb{R}^N , G is $SO(N)$ or $O(N)$, and the Hamiltonian is

$$H(\varphi) = - \sum_{\langle xx' \rangle} a_{xx'} \varphi_x^T \varphi_{x'} \quad (2.14)$$

where $a_{xx'}$ is a real number (usually $a_{xx'} = \beta$ for all $\langle xx' \rangle$). Then the “lifted” Hamiltonian is

$$\widetilde{H}(g) = - \sum_{\langle xx' \rangle} \text{tr}(\alpha_{xx'} g_x^T g_{x'}), \quad (2.15)$$

where

$$\alpha_{xx'} = a_{xx'} \overline{\varphi}_{x'} \overline{\varphi}_x^T \quad (2.16)$$

is an $N \times N$ real matrix of rank 1. This Hamiltonian is of the form (2.5), and so can be handled by the MGMC method described previously.

In this paper we have chosen to study the $SU(2)$ principal chiral model [= N -vector model with $N = 4$] largely because it is easy to implement a heat-bath algorithm on $SU(2) \simeq S^3$ (see Appendix A). The same MGMC principles can be applied to an N -vector model with arbitrary N , but one then needs to devise a heat-bath algorithm on $SO(N)$ or $O(N)$.

MGMC with smooth interpolation. Mack and collaborators [67, 68, 47, 69] have advocated the use of a smooth interpolation (e.g. piecewise-linear or better) in place of piecewise-constant. For fields taking values in a *linear* state space, this is straightforward to do; but for fields taking values in a *nonlinear* manifold (such as a nonlinear σ -model), it is notably awkward: how should one define a fractional power of a group element? The solution proposed by Hasenbusch, Meyer and Mack [47] is to define the coarse-grid update by

$$g_x^{(new)} = \exp(iA_x \Psi) g_x^{(old)}, \quad (2.17)$$

where A_x is a suitable smooth kernel and Ψ is an element of the Lie algebra of G . (More precisely, they take A_x to be the longest-wavelength mode of the Laplace operator on an $\ell_B \times \ell_B$ block with Dirichlet boundary conditions.) Note that here the updates are made in the “unigrid” style [60]: the only field in the problem is the original (finest-grid) field; and the updates (2.17) are performed successively on the 1×1 blocks (in some order), then on the 2×2 blocks, then on the 4×4 blocks, etc. For such an update the labor is proportional to the number of *fine-grid* spins involved in the update, i.e. (2.8) is replaced by

$$W_l \approx W_M, \quad (2.18)$$

so that the total work for one unigrid iteration is

$$\begin{aligned}
\text{work}(UG) &= W_M \sum_{l=M}^0 \gamma^{M-l} \\
&\sim \begin{cases} MW_M & \text{if } \gamma = 1 \\ \gamma^M W_M & \text{if } \gamma > 1 \end{cases} \\
&\sim \begin{cases} L^d \log L & \text{if } \gamma = 1 \\ L^{d+\log_2 \gamma} & \text{if } \gamma > 1 \end{cases} \tag{2.19}
\end{aligned}$$

Thus, the computational complexity per iteration is tolerable only for a V-cycle. Note also that the energy $H(g^{(new)})$ is an extremely complicated function of the Lie-algebra element Ψ , so it is not feasible to choose Ψ by a heat-bath method; rather, Ψ is chosen by the Metropolis prescription with a suitable hit size $\epsilon \sim \ell_B^{-(d-2)/2}$.

It is now natural to ask: what does one gain by the use of a smooth kernel in place of a piecewise-constant kernel? In the Gaussian case the answer was given above: with a smooth kernel critical slowing-down is eliminated already for a V-cycle¹², while with a piecewise-constant kernel a W-cycle is required. However, this fact does not give any advantage to the smooth kernel, since in the piecewise-constant case we can readily implement the W-cycle in a CPU time of order volume, provided that $d > 1$ [see (2.9)]. In the non-Gaussian case it is less clear what will happen, but we are unable to see why a smooth interpolation should handle strongly nonlinear excitations (such as meson-meson scattering or glueball bound states) any better than a piecewise-constant interpolation. We return to these points in Section 4.2.

3 Numerical Results

3.1 Quantities to be Measured

We begin by defining the quantities — autocorrelation functions and autocorrelation times — that characterize the Monte Carlo dynamics. Let A be an observable (i.e. a function of the field configuration g). We are interested in the evolution of A in Monte Carlo time, and more particularly in the rate at which the system “loses memory” of the past. We define, therefore, the *unnormalized autocorrelation function*¹³

$$C_{AA}(t) = \langle A_s A_{s+t} \rangle - \langle A \rangle^2, \tag{3.1}$$

¹² Here “smooth” refers to an interpolation which is piecewise-linear or better, i.e. one in which linear functions are exactly interpolated. It is worth noting that the Hasenbusch-Meyer-Mack kernels [67, 68, 47] do *not* satisfy this property; indeed, not even a constant function can be exactly interpolated. (That is, the constant function cannot be represented as a linear combination of the kernels A_x corresponding to non-overlapping blocks of the same size, with the exception of the cases $\ell_B = 1$ and $\ell_B = 2$.) Therefore, we do not know whether critical slowing-down is completely eliminated (for Gaussians) in the Hasenbusch-Meyer-Mack V-cycle; we suspect that it may not be. In view of the identities in [6, Section VIII], this problem could be studied numerically by measuring the convergence rate of the corresponding *deterministic* MG algorithm for solving Laplace’s equation. (Note, however, that a more recent work by Hasenbusch and Meyer [69] uses piecewise-linear interpolation.)

¹³ In the mathematics and statistics literature, this is called the *autocovariance function*.

where expectations are taken *in equilibrium*. The corresponding *normalized autocorrelation function* is

$$\rho_{AA}(t) = C_{AA}(t)/C_{AA}(0). \quad (3.2)$$

We then define the *integrated autocorrelation time*

$$\begin{aligned} \tau_{int,A} &= \frac{1}{2} \sum_{t=-\infty}^{\infty} \rho_{AA}(t) \\ &= \frac{1}{2} + \sum_{t=1}^{\infty} \rho_{AA}(t) \end{aligned} \quad (3.3)$$

[The factor of $\frac{1}{2}$ is purely a matter of convention; it is inserted so that $\tau_{int,A} \approx \tau$ if $\rho_{AA}(t) \approx e^{-|t|/\tau}$ with $\tau \gg 1$.] The integrated autocorrelation time controls the statistical error in Monte Carlo measurements of $\langle A \rangle$. More precisely, the sample mean

$$\bar{A} \equiv \frac{1}{n} \sum_{t=1}^n A_t \quad (3.4)$$

has variance

$$\begin{aligned} \text{var}(\bar{A}) &= \frac{1}{n^2} \sum_{r,s=1}^n C_{AA}(r-s) \\ &= \frac{1}{n} \sum_{t=-(n-1)}^{n-1} \left(1 - \frac{|t|}{n}\right) C_{AA}(t) \end{aligned} \quad (3.5)$$

$$\approx \frac{1}{n} (2\tau_{int,A}) C_{AA}(0) \quad \text{for } n \gg \tau \quad (3.6)$$

Thus, the variance of \bar{A} is a factor $2\tau_{int,A}$ larger than it would be if the $\{A_t\}$ were statistically independent. Stated differently, the number of “effectively independent samples” in a run of length n is roughly $n/2\tau_{int,A}$. The autocorrelation time $\tau_{int,A}$ (for interesting observables A) is therefore a “figure of (de)merit” of a Monte Carlo algorithm.

We shall measure static quantities (expectations) and dynamic quantities (autocorrelation times) for the following observables:

$$\vec{\mathcal{M}} = \sum_x \boldsymbol{\sigma}_x \quad (3.7)$$

$$\mathcal{M}^2 = \left(\sum_x \boldsymbol{\sigma}_x \right)^2 \quad (3.8)$$

$$\mathcal{F} = \frac{1}{2} \left[\left| \sum_x e^{2\pi i x_1/L} \boldsymbol{\sigma}_x \right|^2 + \left| \sum_x e^{2\pi i x_2/L} \boldsymbol{\sigma}_x \right|^2 \right] \quad (3.9)$$

$$\mathcal{E} = \sum_{\langle xx' \rangle} \boldsymbol{\sigma}_x \cdot \boldsymbol{\sigma}_{x'} \quad (3.10)$$

The mean values of these observables give information on different aspects of the 2-point function

$$G(x) = \langle \boldsymbol{\sigma}_0 \cdot \boldsymbol{\sigma}_x \rangle \quad (3.11a)$$

$$\tilde{G}(p) = \sum_x e^{ip \cdot x} \langle \boldsymbol{\sigma}_0 \cdot \boldsymbol{\sigma}_x \rangle \quad (3.11b)$$

In particular, we are interested in the *susceptibility*

$$\chi = \tilde{G}(0) = V^{-1} \langle \mathcal{M}^2 \rangle \quad (3.12)$$

and the analogous quantity at the smallest nonzero momentum

$$F = \tilde{G}(p)|_{|p|=2\pi/L} = V^{-1} \langle \mathcal{F} \rangle . \quad (3.13)$$

By combining these we can obtain the (*second-moment*) *correlation length*

$$\xi = \left(\frac{(\chi/F) - 1}{4 \sin^2(\pi/L)} \right)^{1/2} \quad (3.14)$$

(see the Remark below). Finally, we have the (negative) *energy*

$$E = 2G(x)|_{|x|=1} = V^{-1} \langle \mathcal{E} \rangle . \quad (3.15)$$

Here $V = L^2$ is the number of sites in the lattice.

Remark. The definition (3.14) is sometimes summarized [42] by saying that we are fitting $\tilde{G}(p)$ to the Ansatz

$$\tilde{G}(p) = Z \left[\xi^{-2} + 4 \sum_{i=1}^d \sin^2(p_i/2) \right]^{-1} \quad (3.16)$$

at $p = 0$ and $|p| = 2\pi/L$. This is of course true; but it is important to emphasize that we are *not* assuming that $\tilde{G}(p)$ really has the free-field form (3.16) at general p (of course it doesn't). Rather, we simply use this form to motivate *one* reasonable definition of the second-moment correlation length ξ on a finite lattice. Another definition — slightly different but equally reasonable — would be

$$\begin{aligned} \xi' &= \left(\frac{\frac{1}{2d} \sum_x \left(\sum_{i=1}^d (L/\pi)^2 \sin^2(\pi x_i/L) \right) G(x)}{\sum_x G(x)} \right)^{1/2} \\ &= \frac{L^2}{4\pi^2} \left(1 - \frac{F}{\chi} \right) . \end{aligned} \quad (3.17)$$

The two definitions coincide in the infinite-volume limit $L \rightarrow \infty$. Finally, let us emphasize that *neither* of these quantities is equal to the exponential correlation length (= 1/mass gap)

$$\xi_{exp} = \lim_{|x| \rightarrow \infty} \frac{-|x|}{\log G(x)} . \quad (3.18)$$

However, ξ (or ξ') and ξ_{exp} are believed to scale in the same way as $\beta \rightarrow \infty$.

The integrated autocorrelation time $\tau_{int,A}$ can be estimated by standard procedures of statistical time-series analysis [70, 71]. These procedures also give statistically valid *error*

$d = 2$ $O(4)$ model at $L = 32$									
β	Type	Sweeps	Disc	χ	ξ	E	$\tau_{int, \vec{\mathcal{M}}}$	$\tau_{int, \mathcal{M}^2}$	
2.00	HB	500000	10000	92.9 (0.4)	7.61(0.03)	1.15499 (0.00006)	66.19 (3.78)	20.68 (0.66)	
2.00	W	100000	5000	93.7 (0.3)	7.67(0.02)	1.15525 (0.00010)	1.19 (0.02)	2.64 (0.07)	
2.10	HB	500000	10000	134.6 (0.5)	9.63(0.03)	1.20400 (0.00005)	108.48 (7.92)	23.23 (0.79)	
2.10	W	100000	5000	134.3 (0.4)	9.61(0.03)	1.20399 (0.00009)	1.33 (0.03)	2.74 (0.07)	
2.20	HB	500000	10000	178.4 (0.6)	11.57(0.04)	1.24789 (0.00005)	145.37 (12.29)	23.97 (0.82)	
2.20	W	100000	5000	178.5 (0.4)	11.60(0.03)	1.24779 (0.00008)	1.46 (0.03)	2.66 (0.07)	
2.30	HB	500000	10000	221.2 (0.5)	13.43(0.04)	1.28684 (0.00004)	213.38 (21.88)	20.37 (0.65)	
2.30	W	100000	5000	221.1 (0.4)	13.41(0.03)	1.28691 (0.00008)	1.57 (0.03)	2.19 (0.05)	
2.40	W	100000	5000	258.5 (0.3)	14.94(0.03)	1.32155 (0.00007)	1.69 (0.04)	1.94 (0.04)	

Table 1: Data for the two-dimensional $O(4)$ model on a 32×32 lattice. “Type” is the method used (heat-bath, V-cycle, W-cycle or super-W-cycle). “Sweeps” is the number of MGMC iterations performed; a heat-bath “iteration” here is equal to two usual heat-bath sweeps. “Disc” is the number of iterations discarded prior to beginning the analysis. Standard error is shown in parentheses.

bars on $\langle A \rangle$ and $\tau_{int, A}$. For more details, see [72, Appendix C]. In this paper we have used a self-consistent truncation window of width $c\tau_{int, A}$, where c is a constant. In most cases we have used $c = 6$; this choice is reasonable whenever the autocorrelation function $\rho_{AA}(t)$ decays roughly exponentially. However, for the energy ($A = \mathcal{E}$) we noticed that $\rho_{AA}(t)$ has a slowly-decaying component with very small amplitude, and taking $c = 6$ led to a systematic underestimate of $\tau_{int, \mathcal{E}}$. Therefore, for $A = \mathcal{E}$ we took $c = 20$ for the heat-bath, $c = 15$ for the V-cycle, and $c = 10$ for the W-cycle and super-W-cycle; this choice seemed to give a reasonable window width.

In setting error bars on ξ we have used the triangle inequality; such error bars are overly conservative, but we did not feel it was worth the trouble to measure the cross-correlations between \mathcal{M}^2 and \mathcal{F} .

3.2 Summary of our Runs

We performed extensive runs using the MGMC algorithm with $\gamma = 0, 1, 2, 3$ (heat-bath, V-cycle, W-cycle and S-cycle, respectively) and $m_1 = m_2 = 1$, on lattices of sizes $L = 32, 64, 128, 256$. We made an extremely detailed effort to study the W-cycle and a moderately detailed effort to study the V-cycle; only a few runs were made to study, for comparison purposes, the heat-bath and the S-cycle. In all cases the coarsest grid is taken to be 2×2 . All runs used a random initial configuration (“hot start”). The results of these computations are shown in Tables 1, 2, 3 and 4. Here $\beta \equiv \beta_{O(4)} = 2\beta_{SU(2)}$. The heat-bath runs use the MGMC program but with a cycle control parameter $\gamma = 0$, so each “iteration” consists of *two* heat-bath sweeps.

In the heat-bath and V-cycle algorithms, the slowest mode (of those we study) is the total magnetization $\vec{\mathcal{M}}$: global spin rotations are very slow. In the W-cycle and S-cycle algorithms, by contrast, the autocorrelation time $\tau_{int, \vec{\mathcal{M}}}$ is negligible: the MGMC algorithm

$d = 2$ $O(4)$ model at $L = 64$								
β	Type	Sweeps	Disc	χ	ξ	E	$\tau_{int, \vec{M}}$	$\tau_{int, \mathcal{M}^2}$
2.10	V	200000	10000	161.2 (0.9)	10.45(0.04)	1.20182 (0.00003)	13.47 (0.56)	8.49 (0.28)
2.10	W	200000	5000	160.0 (0.6)	10.39(0.03)	1.20187 (0.00003)	1.24 (0.02)	3.44 (0.07)
2.15	W	200000	5000	202.9 (0.7)	11.93(0.03)	1.22410 (0.00003)	1.32 (0.02)	3.88 (0.09)
2.20	HB	500000	10000	257.2 (2.3)	13.74(0.09)	1.24532 (0.00002)	217.47 (22.53)	72.96 (4.37)
2.20	V	200000	10000	258.2 (1.5)	13.78(0.06)	1.24527 (0.00003)	18.92 (0.93)	11.30 (0.43)
2.20	W	200000	5000	258.3 (0.9)	13.79(0.04)	1.24533 (0.00003)	1.38 (0.02)	4.39 (0.10)
2.20	S	100000	5000	258.6 (1.1)	13.83(0.04)	1.24534 (0.00004)	0.51 (0.01)	2.89 (0.08)
2.22	W	200000	5000	283.3 (1.0)	14.58(0.04)	1.25349 (0.00003)	1.42 (0.02)	4.58 (0.11)
2.24	W	200000	5000	309.5 (1.0)	15.38(0.04)	1.26149 (0.00003)	1.45 (0.02)	4.58 (0.11)
2.26	W	200000	5000	337.4 (1.1)	16.20(0.04)	1.26932 (0.00003)	1.48 (0.02)	4.71 (0.12)
2.28	W	200000	5000	364.7 (1.2)	16.93(0.04)	1.27692 (0.00003)	1.51 (0.02)	4.79 (0.12)
2.30	HB	500000	10000	393.5 (3.3)	17.71(0.12)	1.28442 (0.00002)	366.26 (49.44)	90.60 (6.04)
2.30	V	200000	10000	395.8 (2.0)	17.83(0.07)	1.28441 (0.00003)	23.84 (1.31)	12.39 (0.49)
2.30	W	200000	5000	395.3 (1.2)	17.82(0.04)	1.28442 (0.00003)	1.52 (0.02)	5.00 (0.13)
2.30	S	100000	5000	394.1 (1.4)	17.79(0.05)	1.28445 (0.00004)	0.52 (0.01)	3.18 (0.09)
2.35	W	200000	5000	471.5 (1.3)	19.87(0.05)	1.30244 (0.00003)	1.60 (0.02)	5.02 (0.13)
2.40	HB	500000	10000	559.1 (3.6)	22.24(0.14)	1.31957 (0.00002)	545.55 (90.06)	93.08 (6.29)
2.40	V	200000	10000	549.3 (2.1)	21.86(0.08)	1.31945 (0.00003)	29.87 (1.84)	12.27 (0.49)
2.40	W	200000	5000	550.0 (1.3)	21.89(0.05)	1.31942 (0.00002)	1.66 (0.02)	4.83 (0.12)
2.40	S	100000	5000	551.9 (1.5)	21.91(0.06)	1.31956 (0.00003)	0.52 (0.01)	3.04 (0.09)
2.43	W	200000	5000	601.5 (1.3)	23.22(0.05)	1.32931 (0.00002)	1.71 (0.03)	4.39 (0.10)
2.45	W	200000	5000	632.5 (1.2)	23.97(0.05)	1.33563 (0.00002)	1.74 (0.03)	4.21 (0.10)
2.50	HB	500000	10000	706.6 (3.8)	25.79(0.16)	1.35092 (0.00002)	713.40 (133.84)	97.46 (6.74)
2.50	V	200000	10000	707.8 (1.9)	25.81(0.08)	1.35092 (0.00002)	35.21 (2.29)	10.14 (0.36)
2.50	W	200000	5000	706.4 (1.2)	25.75(0.05)	1.35093 (0.00002)	1.79 (0.03)	4.00 (0.09)
2.55	W	200000	5000	779.0 (1.1)	27.49(0.05)	1.36545 (0.00002)	1.84 (0.03)	3.45 (0.07)
2.60	W	200000	5000	848.0 (1.1)	29.08(0.05)	1.37928 (0.00002)	1.92 (0.03)	3.27 (0.07)

Table 2: Data for the two-dimensional $O(4)$ model on a 64×64 lattice. “Type” is the method used (heat-bath, V-cycle, W-cycle or super-W-cycle). “Sweeps” is the number of MGMC iterations performed; a heat-bath “iteration” here is equal to two usual heat-bath sweeps. “Disc” is the number of iterations discarded prior to beginning the analysis. Standard error is shown in parentheses.

$d = 2$ $O(4)$ model at $L = 128$								
β	Type	Sweeps	Disc	χ	ξ	E	$\tau_{int, \bar{\mathcal{M}}}$	$\tau_{int, \mathcal{M}^2}$
2.10	W	200000	5000	161.0 (0.6)	10.31(0.03)	1.20177 (0.00002)	1.15 (0.01)	2.55 (0.05)
2.20	V	200000	10000	269.7 (2.0)	14.16(0.07)	1.24508 (0.00002)	20.64 (1.06)	12.50 (0.50)
2.20	W	200000	5000	267.7 (1.1)	13.99(0.04)	1.24509 (0.00001)	1.30 (0.02)	3.57 (0.08)
2.25	W	200000	5000	346.3 (1.5)	16.26(0.05)	1.26504 (0.00001)	1.39 (0.02)	4.34 (0.10)
2.30	V	200000	10000	452.4 (3.9)	19.07(0.11)	1.28394 (0.00001)	28.36 (1.70)	18.79 (0.92)
2.30	W	200000	5000	449.0 (2.0)	18.83(0.06)	1.28395 (0.00001)	1.47 (0.02)	5.08 (0.13)
2.35	W	200000	5000	580.0 (2.7)	21.81(0.07)	1.30186 (0.00001)	1.54 (0.02)	6.02 (0.17)
2.40	V	200000	10000	747.0 (6.8)	25.24(0.16)	1.31885 (0.00001)	39.87 (2.84)	26.50 (1.54)
2.40	W	200000	5000	744.1 (3.4)	25.12(0.08)	1.31887 (0.00001)	1.61 (0.02)	6.56 (0.19)
2.45	W	200000	5000	952.9 (4.3)	29.08(0.10)	1.33499 (0.00001)	1.70 (0.03)	7.61 (0.24)
2.50	V	200000	10000	1172.5 (9.8)	32.60(0.21)	1.35028 (0.00001)	53.35 (4.40)	30.20 (1.87)
2.50	W	200000	5000	1195.9 (4.9)	33.34(0.11)	1.35029 (0.00001)	1.75 (0.03)	7.91 (0.25)
2.50	S	100000	5000	1193.5 (5.4)	33.21(0.11)	1.35031 (0.00002)	0.50 (0.01)	4.48 (0.15)
2.55	W	200000	5000	1463.6 (5.3)	37.66(0.11)	1.36488 (0.00001)	1.82 (0.03)	7.78 (0.24)
2.60	V	200000	10000	1745.9 (11.1)	41.83(0.24)	1.37874 (0.00001)	68.42 (6.37)	30.01 (1.86)
2.60	W	200000	5000	1723.2 (5.6)	41.33(0.12)	1.37875 (0.00001)	1.89 (0.03)	7.72 (0.24)
2.65	W	200000	5000	2003.5 (5.6)	45.39(0.12)	1.39195 (0.00001)	1.95 (0.03)	7.21 (0.22)
2.70	V	200000	10000	2290.0 (10.8)	49.53(0.25)	1.40459 (0.00001)	73.51 (7.10)	25.73 (1.47)
2.70	W	200000	5000	2294.7 (5.2)	49.61(0.12)	1.40460 (0.00001)	1.99 (0.03)	6.23 (0.18)
2.75	W	200000	5000	2561.3 (5.0)	53.26(0.12)	1.41666 (0.00001)	2.06 (0.03)	5.94 (0.16)
2.80	W	200000	5000	2813.8 (4.6)	56.54(0.11)	1.42821 (0.00001)	2.14 (0.04)	5.12 (0.13)

Table 3: Data for the two-dimensional $O(4)$ model on a 128×128 lattice. “Type” is the method used (heat-bath, V-cycle, W-cycle or super-W-cycle). “Sweeps” is the number of MGMC iterations performed; a heat-bath “iteration” here is equal to two usual heat-bath sweeps. “Disc” is the number of iterations discarded prior to beginning the analysis. Standard error is shown in parentheses.

$d = 2$ $O(4)$ model at $L = 256$								
β	Type	Sweeps	Disc	χ	ξ	E	$\tau_{int, \vec{\mathcal{M}}}$	$\tau_{int, \mathcal{M}^2}$
2.50	V	200000	10000	1316.2 (16.6)	34.80(0.30)	1.35021 (0.00001)	65.79 (6.01)	37.72 (2.61)
2.50	W	100000	5000	1319.0 (10.2)	35.04(0.19)	1.35021 (0.00001)	1.66 (0.04)	7.13 (0.31)
2.60	V	200000	10000	2240.7 (30.1)	46.77(0.44)	1.37859 (0.00001)	86.32 (9.04)	53.02 (4.35)
2.60	W	200000	5000	2229.4 (12.8)	46.64(0.19)	1.37860 (0.00001)	1.84 (0.03)	9.80 (0.34)
2.70	V	200000	10000	3648.7 (45.2)	61.76(0.59)	1.40444 (0.00001)	113.19 (13.59)	62.62 (5.58)
2.70	W	200000	5000	3646.8 (19.3)	61.92(0.25)	1.40443 (0.00000)	1.98 (0.03)	11.55 (0.44)
2.80	V	200000	10000	5519.2 (54.3)	79.39(0.71)	1.42806 (0.00000)	141.24 (18.91)	64.76 (5.86)
2.80	W	200000	5000	5448.7 (23.4)	78.33(0.29)	1.42806 (0.00000)	2.12 (0.04)	11.59 (0.44)
3.00	W	100000	5000	9300.0 (30.2)	108.21(0.41)	1.46979 (0.00001)	2.31 (0.06)	8.24 (0.38)

Table 4: Data for the two-dimensional $O(4)$ model on a 256×256 lattice. “Type” is the method used (heat-bath, V-cycle, W-cycle or super-W-cycle). “Sweeps” is the number of MGMC iterations performed; a heat-bath “iteration” here is equal to two usual heat-bath sweeps. “Disc” is the number of iterations discarded prior to beginning the analysis. Standard error is shown in parentheses.

performs global spin rotations very efficiently. Indeed, if we had taken our coarsest grid to be 1×1 instead of 2×2 , then the sequence $\{\vec{\mathcal{M}}_t\}$ would be completely uncorrelated, i.e. $\tau_{int, \vec{\mathcal{M}}} = \frac{1}{2}$ for all β, L .

Of greater physical interest is the squared magnetization \mathcal{M}^2 , which corresponds to *relative* rotations of the spins in different parts of the lattice; this mode is very slow (though not the slowest) in the heat-bath and V-cycle algorithms, and it is essentially the slowest mode of the W-cycle and S-cycle algorithms. For all these algorithms the autocorrelation time $\tau_{int, \mathcal{M}^2}$ has the same qualitative behavior: as a function of β it first rises to a peak and then falls; the location of this peak shifts towards $\beta = \infty$ as L increases; and the height of this peak grows as L increases. In Section 3.4 we shall make a detailed finite-size-scaling analysis of these data.

The autocorrelation time of the energy, $\tau_{int, \mathcal{E}}$, is uniformly small: less than about 2.5 for the heat bath, and less than about 1 for the other cycles. So we do not bother to report it here.

In Tables 5 and 6 we summarize, for the convenience of the reader, our best estimates of the static quantities χ , ξ and E on lattices of size $L = 32, 64, 128, 256$. These estimates come from merging all of the data in Tables 1–4 together with the data from our Wolff-Swendsen-Wang runs [42, 49].¹⁴ These data are consistent with those of Heller [40] and Wolff [46]. We use these merged data in our finite-size-scaling analyses whenever χ and/or ξ is required.

¹⁴ The $L = 256, \beta = 2.60, 2.80$ data from [42] are unreliable due to an observed metastability, and the $L = 32, 64, \beta = 2.20, N_{hit} = 1$ data from [49] are unreliable due to possibly insufficient equilibration; these data points are *not* included in the means. In all other cases, χ, ξ and E from the different algorithms agree within error bars; this is strong evidence that all the programs are correct!

Merged $O(4)$ -Model Static Data				
L	β	χ	ξ	E
32	1.62	21.0 (0.1)	3.09 (0.02)	0.93417 (0.00054)
32	1.70	27.8 (0.0)	3.65 (0.01)	0.98418 (0.00011)
32	1.80	41.3 (0.0)	4.67 (0.01)	1.04456 (0.00007)
32	1.90	62.1 (0.1)	5.96 (0.01)	1.10161 (0.00007)
32	2.00	93.7 (0.1)	7.68 (0.01)	1.15509 (0.00004)
32	2.10	134.6 (0.2)	9.63 (0.01)	1.20398 (0.00004)
32	2.20	178.8 (0.2)	11.60 (0.02)	1.24787 (0.00004)
32	2.30	221.1 (0.3)	13.42 (0.02)	1.28685 (0.00004)
32	2.40	258.5 (0.3)	14.94 (0.03)	1.32155 (0.00007)
32	2.60	322.4 (1.0)	17.50 (0.10)	
32	3.00	418.0 (0.9)	21.30 (0.10)	
32	3.40	488.1 (0.8)	24.30 (0.10)	
64	1.70	27.9 (0.2)	3.65 (0.02)	
64	1.80	41.2 (0.3)	4.60 (0.10)	
64	1.90	64.1 (0.5)	6.10 (0.10)	
64	2.00	99.4 (0.2)	7.83 (0.01)	1.15378 (0.00004)
64	2.10	160.5 (0.3)	10.40 (0.01)	1.20184 (0.00002)
64	2.15	202.9 (0.7)	11.93 (0.03)	1.22410 (0.00003)
64	2.20	257.9 (0.4)	13.77 (0.02)	1.24532 (0.00001)
64	2.22	283.3 (1.0)	14.58 (0.04)	1.25349 (0.00003)
64	2.24	309.5 (1.0)	15.38 (0.04)	1.26149 (0.00003)
64	2.26	337.4 (1.1)	16.20 (0.04)	1.26932 (0.00003)
64	2.28	364.7 (1.2)	16.93 (0.04)	1.27692 (0.00003)
64	2.30	395.0 (0.7)	17.81 (0.03)	1.28442 (0.00001)
64	2.35	471.5 (1.3)	19.87 (0.05)	1.30244 (0.00003)
64	2.40	551.6 (0.8)	21.92 (0.03)	1.31950 (0.00001)
64	2.43	601.5 (1.3)	23.22 (0.05)	1.32931 (0.00002)
64	2.45	632.5 (1.2)	23.97 (0.05)	1.33563 (0.00002)
64	2.50	706.7 (0.9)	25.77 (0.04)	1.35092 (0.00001)
64	2.55	779.0 (1.1)	27.49 (0.05)	1.36545 (0.00002)
64	2.60	847.9 (1.0)	29.06 (0.04)	1.37928 (0.00002)
64	3.00	1286.6 (3.0)	38.40 (0.20)	
64	3.40	1611.5 (2.9)	45.50 (0.20)	
64	3.80	1865.7 (2.7)	51.30 (0.20)	

Table 5: Best estimates of susceptibility, correlation length and energy for the $O(4)$ model on 32×32 and 64×64 lattices, from Tables 1, 2 and [42, 49]. Standard error is shown in parentheses.

Merged $O(4)$ -Model Static Data				
L	β	χ	ξ	E
128	2.00	99.3 (0.8)	7.80 (0.10)	
128	2.10	161.1 (0.5)	10.32 (0.03)	1.20177 (0.00002)
128	2.20	267.9 (0.9)	14.02 (0.03)	1.24509 (0.00001)
128	2.25	346.3 (1.5)	16.26 (0.05)	1.26504 (0.00001)
128	2.30	450.6 (1.6)	18.91 (0.05)	1.28394 (0.00001)
128	2.35	580.0 (2.7)	21.81 (0.07)	1.30186 (0.00001)
128	2.40	745.1 (2.7)	25.15 (0.07)	1.31886 (0.00001)
128	2.45	952.9 (4.3)	29.08 (0.10)	1.33499 (0.00001)
128	2.50	1192.1 (3.4)	33.19 (0.07)	1.35029 (0.00001)
128	2.55	1463.6 (5.3)	37.66 (0.11)	1.36488 (0.00001)
128	2.60	1726.8 (4.6)	41.38 (0.09)	1.37874 (0.00001)
128	2.65	2003.5 (5.6)	45.39 (0.12)	1.39195 (0.00001)
128	2.70	2293.8 (4.7)	49.60 (0.11)	1.40460 (0.00001)
128	2.75	2561.3 (5.0)	53.26 (0.12)	1.41666 (0.00001)
128	2.80	2813.8 (4.6)	56.54 (0.11)	1.42821 (0.00001)
128	3.00	3715.8 (10.6)	67.40 (0.30)	
128	3.40	5124.0 (10.5)	82.50 (0.40)	
256	2.20	267.8 (2.0)	13.70 (0.10)	
256	2.40	765.3 (6.3)	25.50 (0.20)	
256	2.50	1318.2 (8.7)	34.97 (0.16)	1.35021 (0.00001)
256	2.60	2231.1 (11.8)	46.66 (0.17)	1.37860 (0.00001)
256	2.70	3647.1 (17.7)	61.90 (0.23)	1.40443 (0.00001)
256	2.80	5459.7 (21.5)	78.48 (0.27)	1.42806 (0.00001)
256	3.00	9300.0 (30.2)	108.21 (0.41)	1.46979 (0.00001)

Table 6: Best estimates of susceptibility, correlation length and energy for the $O(4)$ model on 128×128 and 256×256 lattices, from Tables 3, 4 and [42, 49]. Standard error is shown in parentheses.

3.3 Finite-Size-Scaling Analysis: Static Quantities

In this subsection and the next, we make our conclusions more quantitative by performing a finite-size-scaling analysis.

We fit $\xi(\beta, L)$ to the two-loop asymptotic-freedom finite-size-scaling prediction (1.12) by plotting $\xi\beta^{1/2}e^{-\pi\beta}$ versus ξ/L (Figure 2). Likewise, we fit $\chi(\beta, L)$ to the prediction (1.13) by plotting $\chi\beta^{5/2}e^{-2\pi\beta}$ versus ξ/L (Figure 3). In both cases the points fall quite nicely on a single curve, with the exception of the data points at $\beta \lesssim 2.0$ ($\xi \lesssim 8$). Note also that the scaling curves drop precipitously for $\xi/L \gtrsim 0.4$ (corresponding to $\xi_\infty/L \gtrsim 0.5$); thus, only those points with $\xi/L \lesssim 0.4$ bear much relation to the infinite-volume physics. By extrapolating the scaling curves to $\xi/L = 0$, we can estimate the constants C_ξ and C_χ defined in (1.4)/(1.5):

$$C_{\xi(2\text{-loop})} = (1.93 \pm 0.10) \times 10^{-2} \quad (3.19a)$$

$$C_{\chi(2\text{-loop})} = (1.88 \pm 0.08) \times 10^{-3} \quad (3.19b)$$

(subjective 68% confidence intervals). Unfortunately, this value of C_ξ cannot be directly compared with the exact value $C_\xi = 2.349109\dots \times 10^{-2}$ predicted by the Bethe Ansatz [cf. (1.6)], because we use the second-moment definition of ξ [cf. (3.14)] while the Bethe-Ansatz work [17, 18, 19] uses the exponential definition (= inverse mass gap). However, it is found empirically that the two definitions of ξ agree to within less than 1% — compare our Tables 5 and 6 with Table 1 of [46] — and it would be very interesting to understand *why* this is so!

Finally, it should be noted from Tables 5 and 6 that the finite-size corrections to ξ and χ at fixed β are of order 1–2% when $L \approx 6\xi$ ($\approx 6\xi_\infty$); this finite-size effect should be taken into account in future high-precision work.

The three-loop correction terms a_1 and b_1 in (1.4)/(1.5) have been computed by Falcioni and Treves [26]: they are

$$a_1 = -\frac{1}{2\pi(N-2)} [1 - (N-2)h_1 - h_2] \quad (3.20a)$$

$$b_1 = -\frac{1}{2\pi(N-2)} [2 - 2(N-2)h_1 - 2h_2 + (N-1)(1-k)] \quad (3.20b)$$

where h_1 , h_2 and k can be computed by evaluating lattice Feynman diagrams; for the nearest-neighbor action (1.1) they are $h_1 \approx -0.09$, $h_2 \approx 0.52$, $k \approx 1.57$. Thus, for $N = 4$ we have $a_1 \approx -0.053$ and $b_1 \approx 0.031$. As already noted by Falcioni and Treves for the case $N = 3$, these corrections are too small to affect much the quality of the fit in Figures 2 and 3. However, they do affect the estimates of C_ξ and C_χ by a few percent:

$$C_{\xi(3\text{-loop})} \approx C_{\xi(2\text{-loop})} \times \left(1 + \frac{0.053}{\beta_{av}}\right) \quad (3.21a)$$

$$C_{\chi(3\text{-loop})} \approx C_{\chi(2\text{-loop})} \times \left(1 - \frac{0.031}{\beta_{av}}\right) \quad (3.21b)$$

where $\beta_{av} \approx 2.4$ is an average value of β among those data points contributing to the estimates of C_ξ and C_χ (i.e. $L = 128, 256$ and $\xi/L \lesssim 0.2$). Hence our best estimates for C_ξ

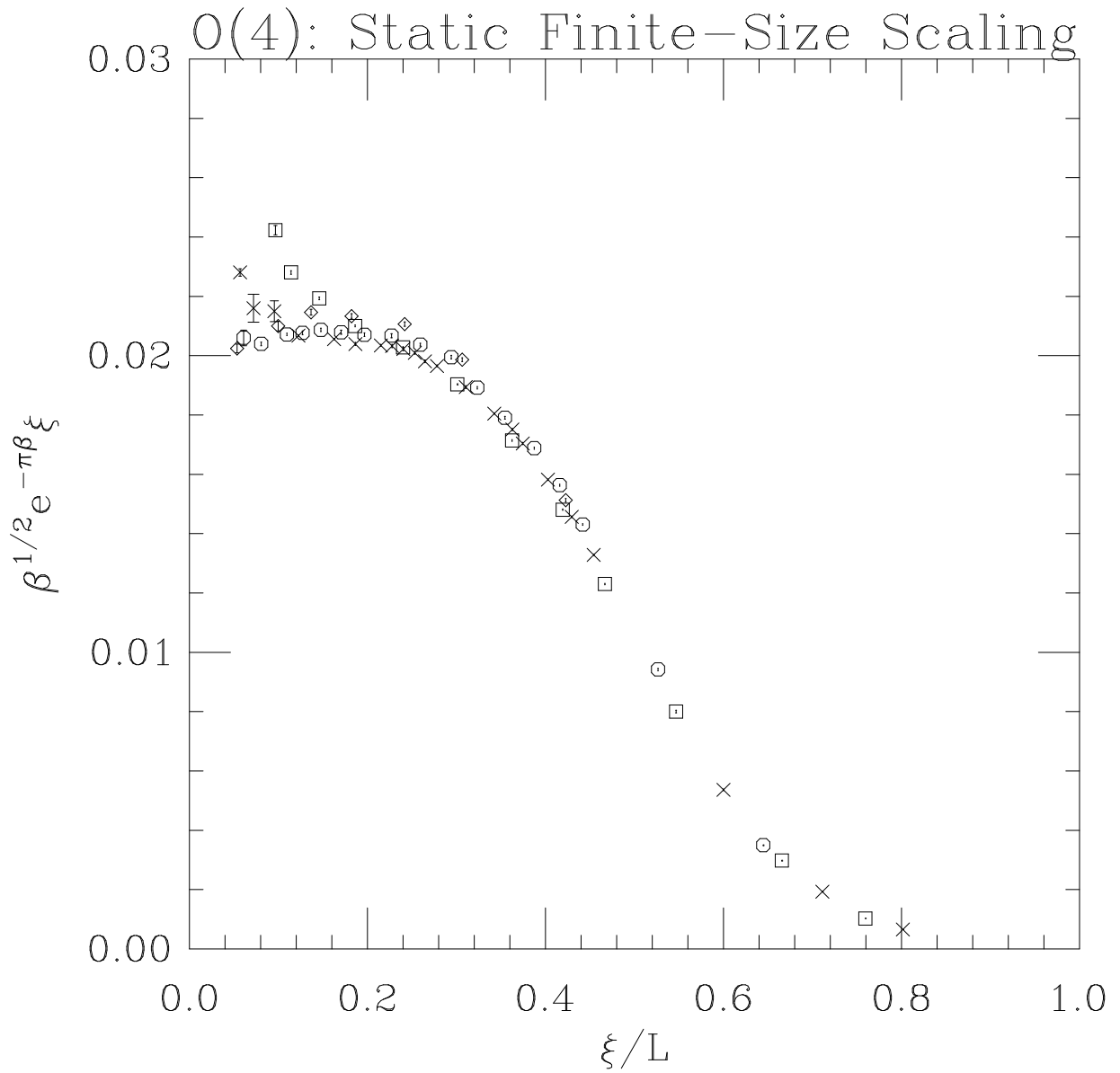


Figure 2: Finite-size-scaling plot of $\beta^{1/2}e^{-\pi\beta\xi}$ versus ξ/L , for lattice sizes $L = 32$ (\square), 64 (\times), 128 (\circ), 256 (\diamond). Error bars are in most cases invisible.

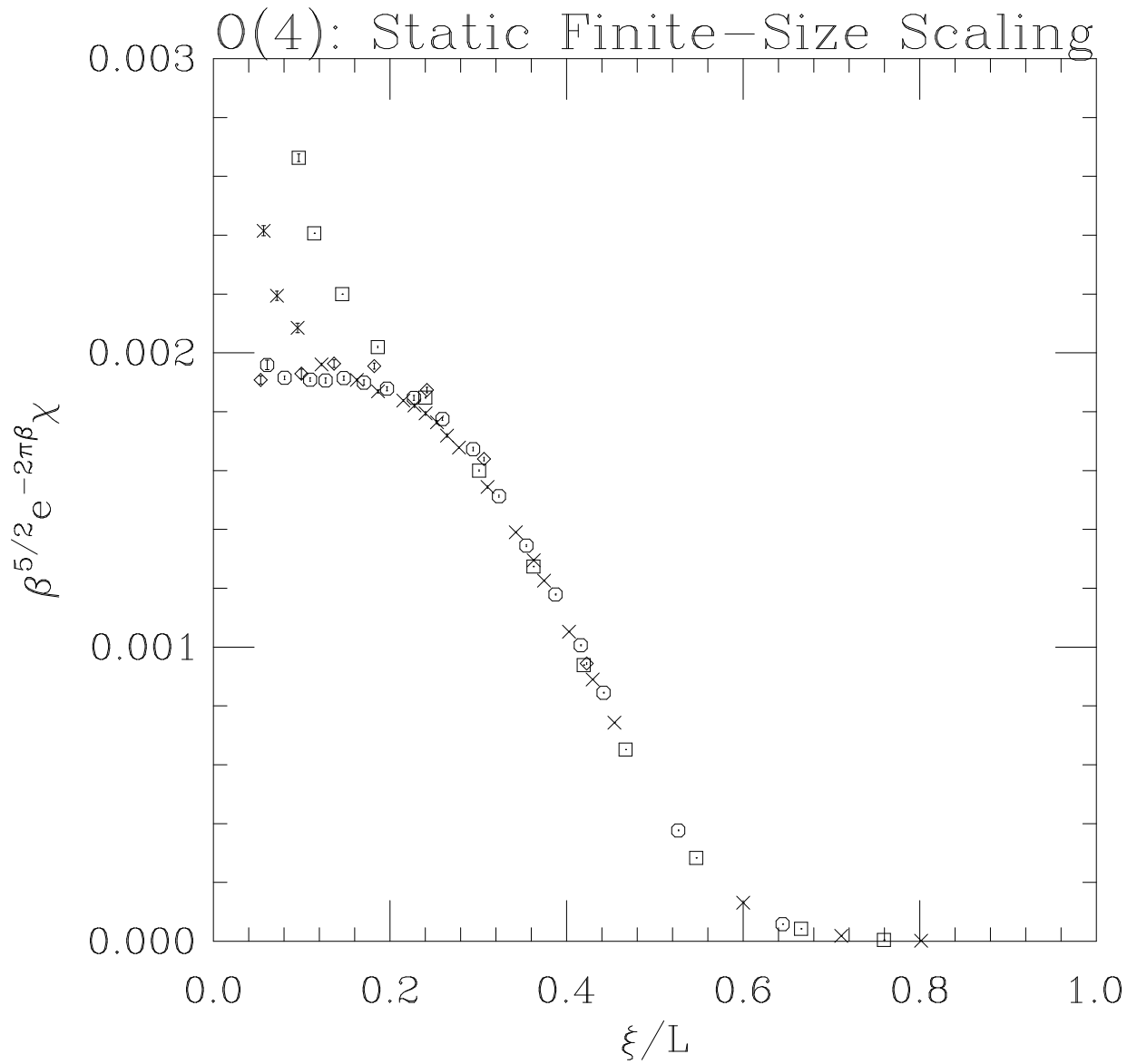


Figure 3: Finite-size-scaling plot of $\beta^{5/2} e^{-2\pi\beta} \chi$ versus ξ/L , for lattice sizes $L = 32$ (\square), 64 (\times), 128 (\circ), 256 (\diamond). Error bars are in most cases invisible.

and C_χ are

$$C_{\xi(3\text{-loop})} = (1.97 \pm 0.10) \times 10^{-2} \quad (3.22a)$$

$$C_{\chi(3\text{-loop})} = (1.86 \pm 0.08) \times 10^{-3} \quad (3.22b)$$

(subjective 68% confidence intervals). Unless the higher-order correction coefficients $a_2, a_3, \dots, b_2, b_3, \dots$ turn out to be surprisingly large, the deviations from scaling observed for $\xi \lesssim 8$ will have to be ascribed to nonperturbative effects.

We also tried to fit χ and ξ to the prediction (1.14) by plotting $\chi\xi^{-2}(\log\xi)^{3/2}$ versus ξ/L . However, the fit was rather poor (see Figure 4); and it was not noticeably improved by including the universal correction term $c_{11} \log \log \xi / \log \xi$ from (1.7). Apparently the trouble is that $|\log C_\xi|$ is comparable in magnitude to $\log \xi$ for the range of temperatures considered here (both are ≈ 4), so the correction term $c_{01}/\log \xi$ is quite significant (and higher-order corrections may also be significant).

In any case, our data show quite good agreement — as good as one has a right to expect for this range of β — with the two-loop and three-loop asymptotic-freedom predictions.

Recently, however, Patrascioiu, Seiler and collaborators [54, 56] have argued on theoretical grounds that non-Abelian σ -models in two dimensions should have a conventional power-law critical point at *finite* β — in sharp contrast to the conventional wisdom (1.4)–(1.14). Moreover, they have claimed to find evidence of such a critical point in a Monte Carlo study [55] of the dodecahedron model (a discrete-spin model that is expected to fall in the universality class of the $O(4)$ -symmetric nonlinear σ -model) on lattices of size up to $L = 80$: their best estimates of the critical exponents are $\nu \approx 2.02$ and $\gamma \approx 3.29$ (with uncertainty of order ± 0.1) and thus $2 - \eta = \gamma/\nu \approx 1.627$. We therefore attempted to fit our data for ξ and χ to the finite-size-scaling forms

$$\xi(\beta, L) \sim L f_\xi((\beta - \beta_c)L^{1/\nu}) \quad (3.23)$$

$$\chi(\beta, L) \sim L^{\gamma/\nu} f_\chi((\beta - \beta_c)L^{1/\nu}) \quad (3.24)$$

We also fit our data to the Ansatz

$$\chi(\beta, L) \sim \xi^{\gamma/\nu} f_{\chi\xi}(\xi/L) \quad (3.25)$$

[where $\xi \equiv \xi(\beta, L)$ and $\lim_{x \rightarrow 0} f_{\chi\xi}(x) = C_{\chi\xi} > 0$], which follows from (3.23)/(3.24) by eliminating β . This latter Ansatz does not test the existence of a power-law critical point at finite β , but rather tests the value of the exponent γ/ν without needing to estimate β_c .

First we attempted a fit to (3.25) by plotting $\chi\xi^{-\gamma/\nu}$ versus ξ/L for a variety of values of γ/ν . We were unable to obtain a satisfactory fit for any choice of γ/ν . In particular, the Patrascioiu-Seiler value $\gamma/\nu = 1.627$ leads to an extremely poor fit. The least poor fit was found at $\gamma/\nu \approx 1.78$; it is shown in Figure 5. However, we do not feel entitled to interpret the inadequacy of these fits as evidence against the Ansatz (3.25), because the fit to the corresponding asymptotic-freedom Ansatz (1.14) was equally poor.

Next we attempted fits to (3.23) and (3.24), which have two and three free parameters, respectively. We began by imposing the Patrascioiu-Seiler values $\nu = 2.02$ and $\gamma = 3.29$ and varying β_c until we obtained the best fit; the results are shown in Figure 6. We see that at $\beta \lesssim 2.1 - 2.3$ (corresponding to $\xi \lesssim 10 - 19$), the fits are reasonable. However, there are

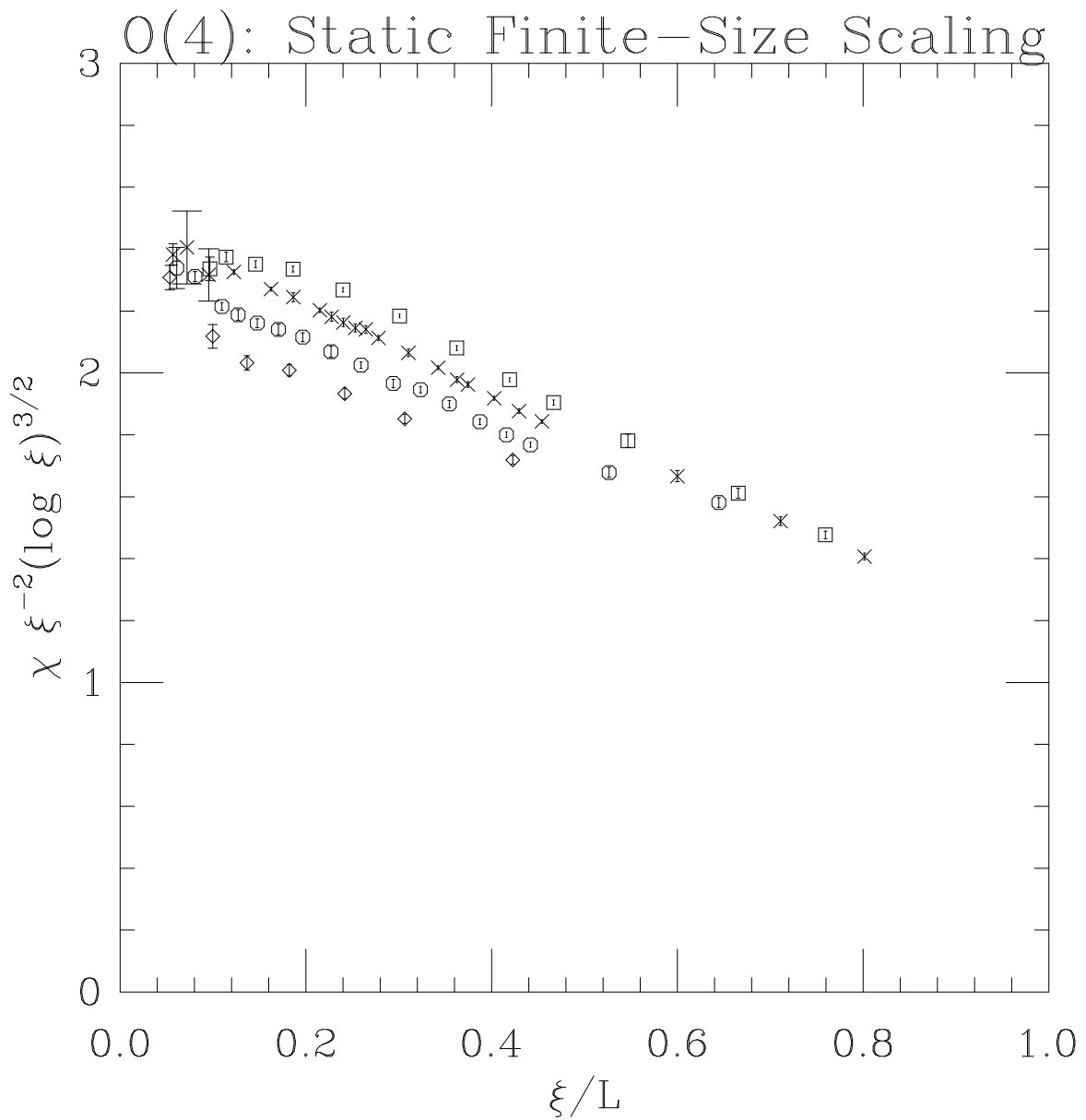


Figure 4: Finite-size-scaling plot of $\chi \xi^{-2} (\log \xi)^{3/2}$ versus ξ/L , for lattice sizes $L = 32$ (\square), 64 (\times), 128 (\circ), 256 (\diamond). Error bars are in most cases invisible.

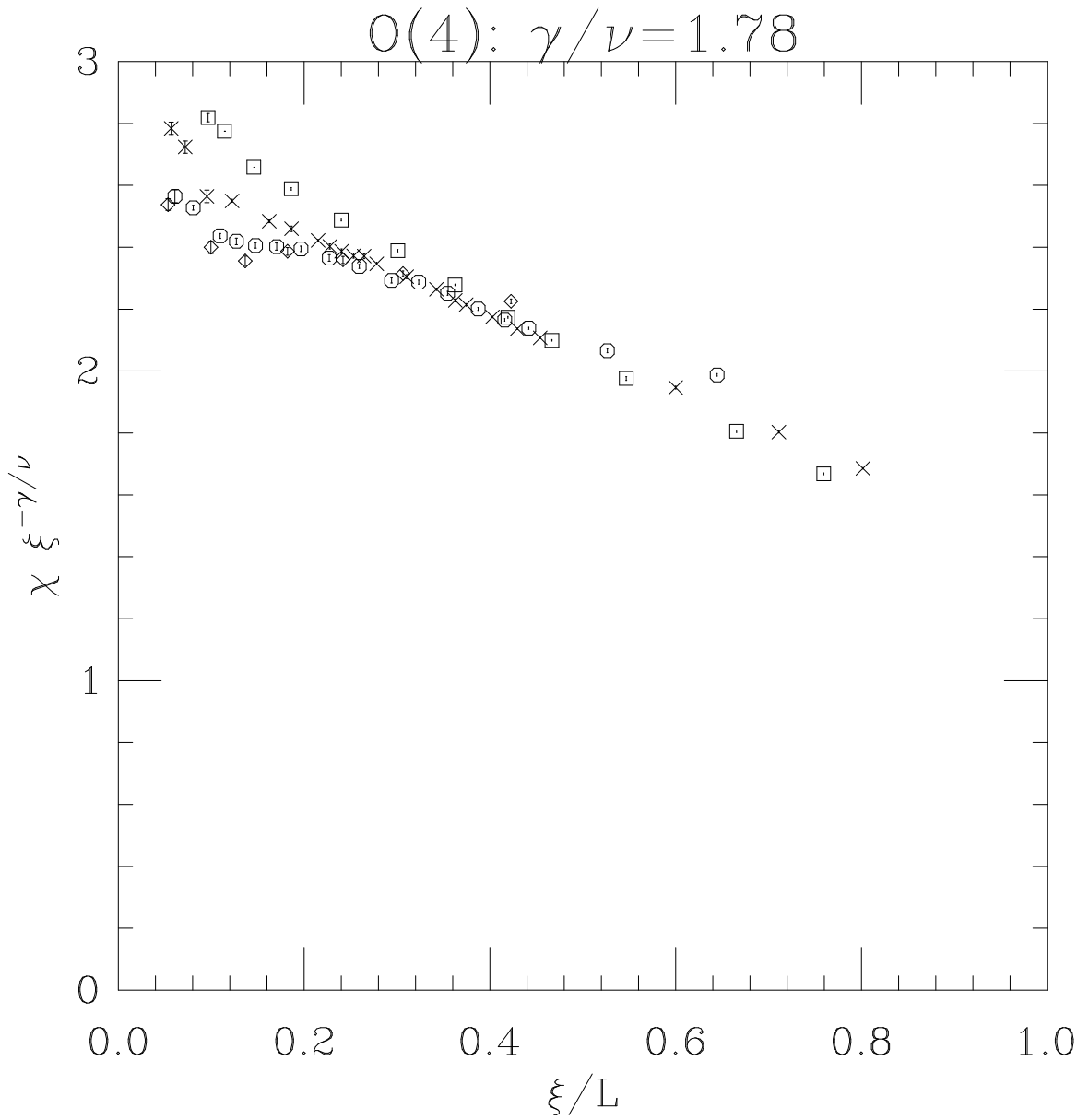


Figure 5: Finite-size-scaling plot of $\chi \xi^{-\gamma/\nu}$ versus ξ/L , for lattice sizes $L = 32$ (\square), 64 (\times), 128 (\circ), 256 (\diamond). Here $\gamma/\nu = 1.78$. Error bars are in most cases invisible.

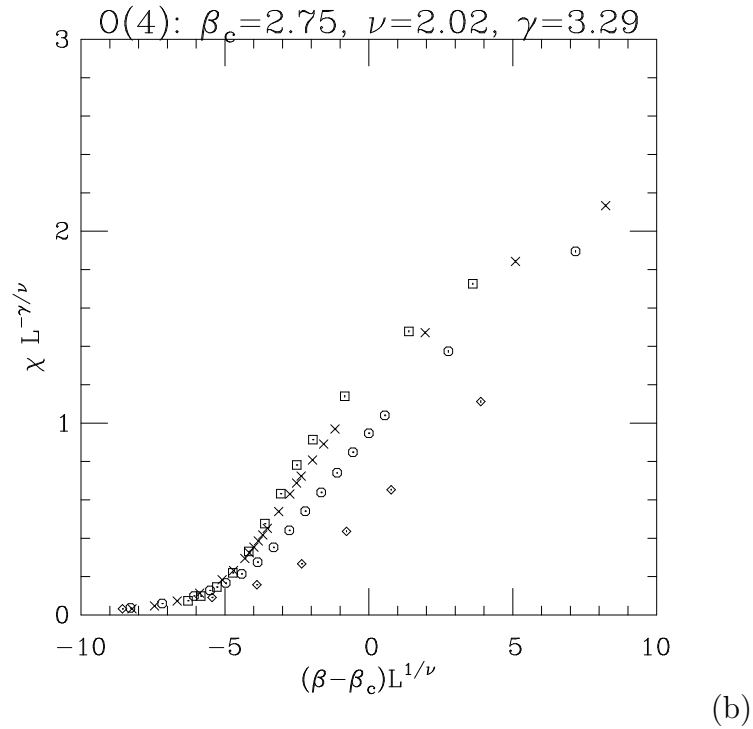
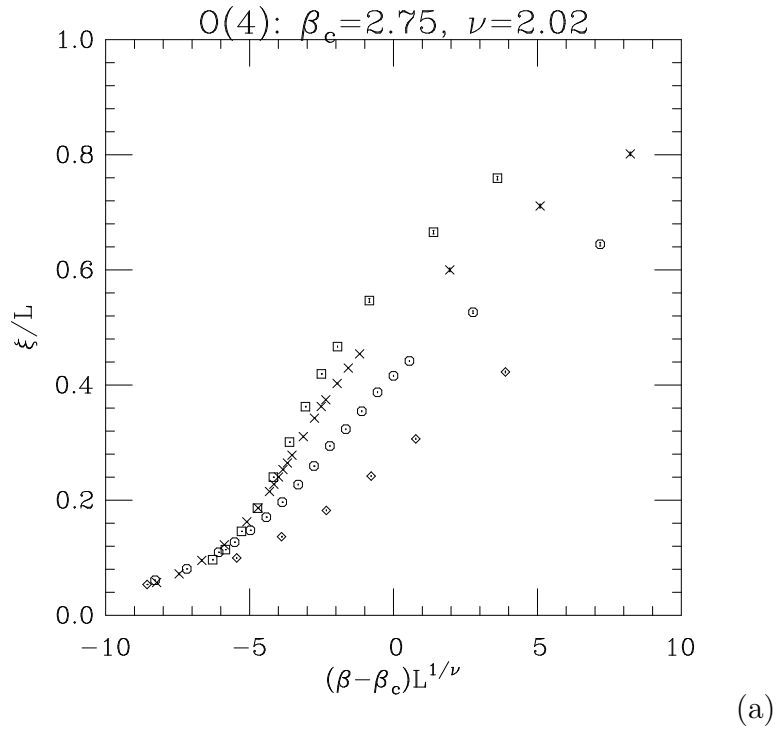


Figure 6: Finite-size-scaling plot of ξ/L (a) and $\chi L^{-\gamma/\nu}$ (b) versus $(\beta - \beta_c)L^{1/\nu}$, for lattice sizes $L = 32$ (\square), 64 (\times), 128 (\circ), 256 (\diamond). Here $\beta_c = 2.75$; values of $\nu = 2.02$ and $\gamma = 3.29$ are taken from ref. [55]. Error bars are in most cases invisible.

very large deviations at larger values of β , which cannot be removed simply by varying β_c . Therefore we tried an unbiased study: at each of various trial values of β_c , we first varied ν until we obtained the best fit to (3.23); then we fixed this value of ν and varied γ until we obtained the best fit to (3.24). Some typical results are shown in Figures 7 ($\beta_c = 3$), 8 ($\beta_c = 4$), 9 ($\beta_c = 5$), and 10 ($\beta_c = 10$). For the smaller values of β_c , the fit is still rather poor; as β_c is raised, the fit remains good out to larger values of β . Moreover, the optimal values of ν and γ grow rapidly with β_c : they are in fact very roughly proportional to β_c (or rather, to $\beta_c - \text{const}$ with $\text{const} \approx 2$). This is exactly the behavior one would expect if the asymptotic-freedom Ansatz (1.4)–(1.14) holds, since a power-law critical point at large β_c and with an exponent proportional to β_c can mimic (for β considerably smaller than β_c) an exponential growth:

$$\left(1 - \frac{\beta}{\beta_c}\right)^{-C\beta_c} = e^{C\beta} \left[1 + \frac{\beta}{2\beta_c} + O\left(\left(\frac{\beta}{\beta_c}\right)^2\right)\right]. \quad (3.26)$$

We believe that our data rule out a power-law critical point for $\beta_c \lesssim 5$ (a value well beyond the betas at which we ran); and our data are compatible with a power-law critical point at $\beta_c \gtrsim 5$ only if one assumes implausibly large values of ν and γ . We conclude that the two-dimensional $O(4)$ model almost certainly does *not* have a power-law critical point at finite β .

3.4 Finite-Size-Scaling Analysis: Dynamic Quantities

Next we apply finite-size scaling to the dynamic quantities $\tau_{int, \vec{\mathcal{M}}}$ and $\tau_{int, \mathcal{M}^2}$. We use the Ansatz

$$\tau_{int, A}(\beta, L) \sim \xi(\beta, L)^{z_{int, A}} g_A(\xi(\beta, L)/L) \quad (3.27)$$

for $A = \vec{\mathcal{M}}, \mathcal{M}^2$. Here g_A is an unknown scaling function, and $g_A(0) = \lim_{x \downarrow 0} g_A(x)$ is supposed to be finite and nonzero.¹⁵ We determine $z_{int, A}$ by plotting $\tau_{int, A} \xi^{-z_{int, A}}$ versus ξ/L and adjusting $z_{int, A}$ until the points fall as closely as possible onto a single curve (with priority to the larger L values). We emphasize that the dynamic critical exponent $z_{int, A}$ is in general *different* from the exponent z_{exp} associated with the exponential autocorrelation time τ_{exp} [1, 73, 4].

Let us begin with $\tau_{int, \mathcal{M}^2}$. Using the procedure just described, we find

$$z_{int, \mathcal{M}^2} = \begin{cases} 2.0 \pm 0.15 & \text{for the heat-bath} \\ 1.13 \pm 0.11 & \text{for the V-cycle} \\ 0.60 \pm 0.07 & \text{for the W-cycle} \\ 0.53 \pm 0.10 & \text{for the S-cycle} \end{cases} \quad (3.28)$$

¹⁵ It is of course equivalent to use the Ansatz

$$\tau_{int, A}(\beta, L) \sim L^{z_{int, A}} h_A(\xi(\beta, L)/L),$$

and indeed the two Ansätze are related by $h_A(x) = x^{z_{int, A}} g_A(x)$. However, to determine whether $\lim_{x \downarrow 0} g_A(x) = \lim_{x \downarrow 0} x^{-z_{int, A}} h_A(x)$ is nonzero, it is more convenient to inspect a graph of g_A than one of h_A .

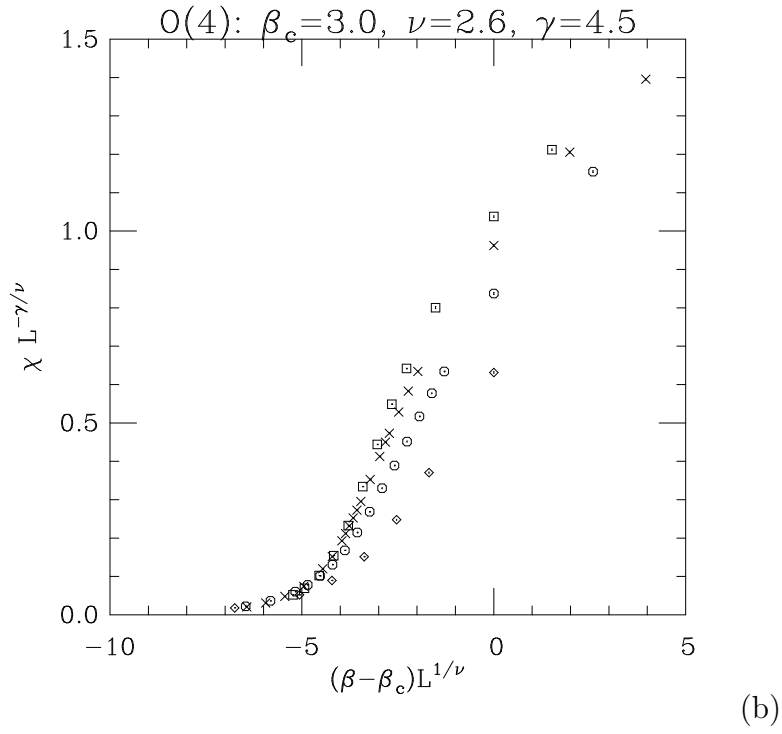
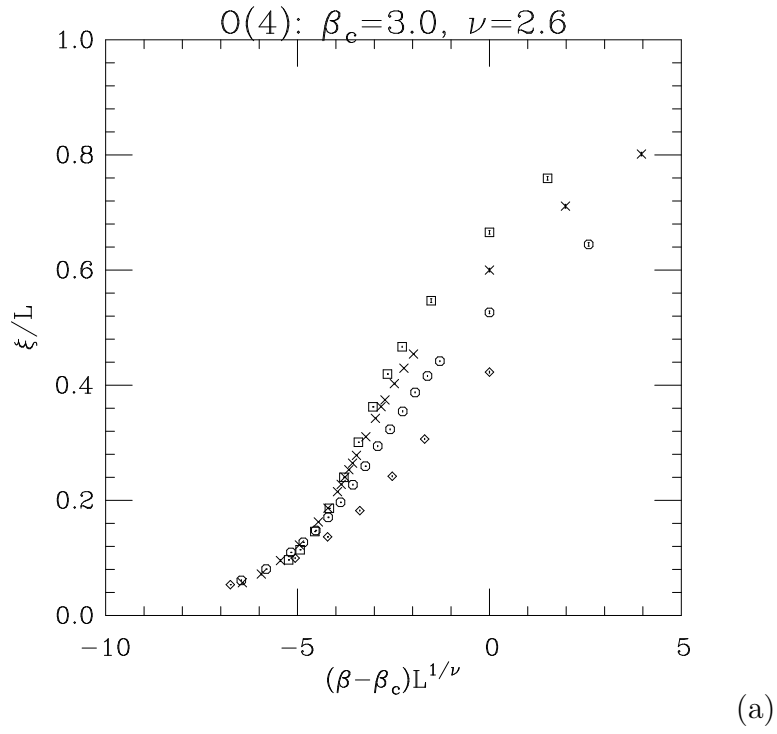


Figure 7: Finite-size-scaling plot of ξ/L (a) and $\chi L^{-\gamma/\nu}$ (b) versus $(\beta - \beta_c)L^{1/\nu}$, for lattice sizes $L = 32$ (\square), 64 (\times), 128 (\circ), 256 (\diamond). Here $\beta_c = 3.0$, $\nu = 2.6$ and $\gamma = 4.5$. Error bars are in most cases invisible.

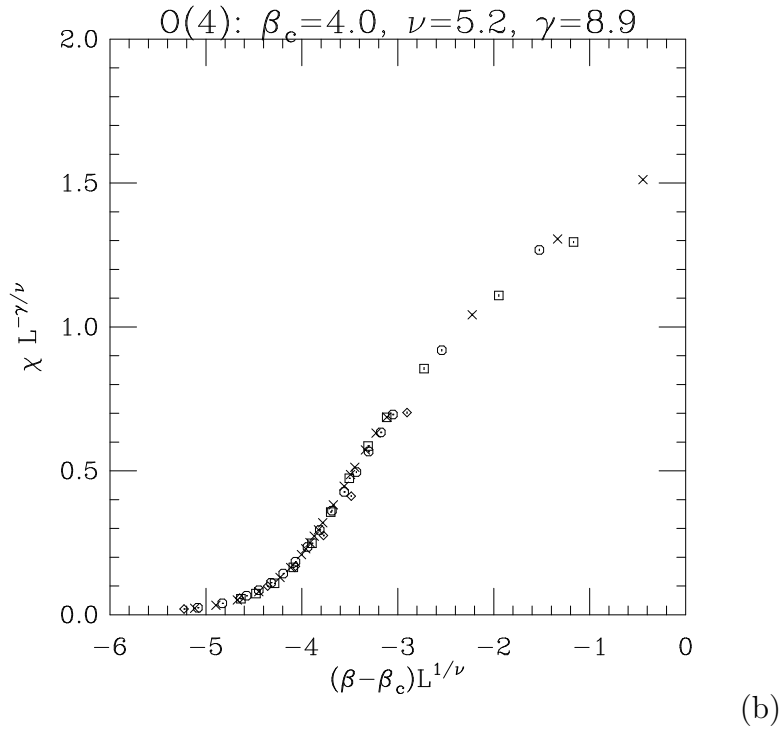
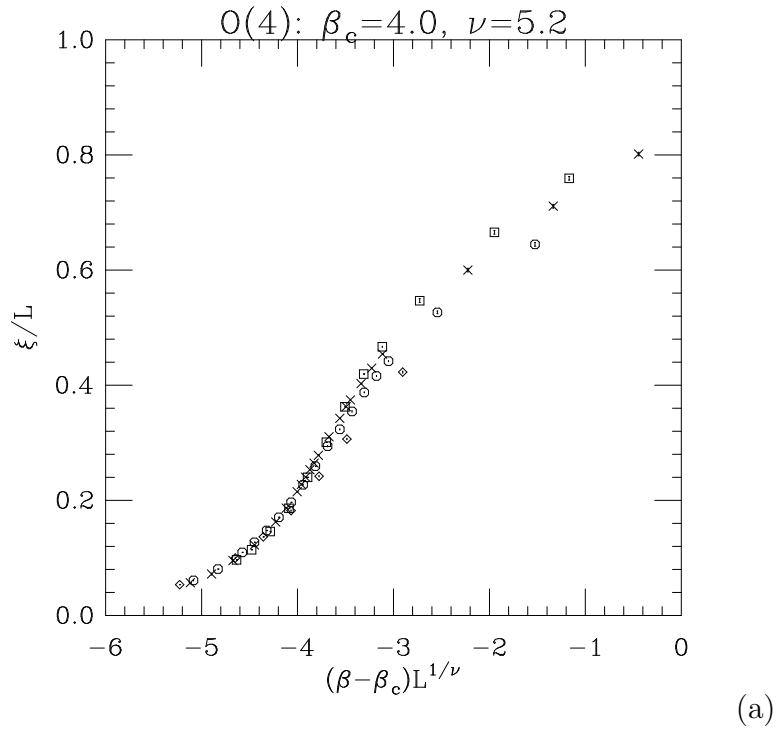


Figure 8: Finite-size-scaling plot of ξ/L (a) and $\chi L^{-\gamma/\nu}$ (b) versus $(\beta - \beta_c)L^{1/\nu}$, for lattice sizes $L = 32$ (\square), 64 (\times), 128 (\circ), 256 (\diamond). Here $\beta_c = 4.0$, $\nu = 5.2$ and $\gamma = 8.9$. Error bars are in most cases invisible.

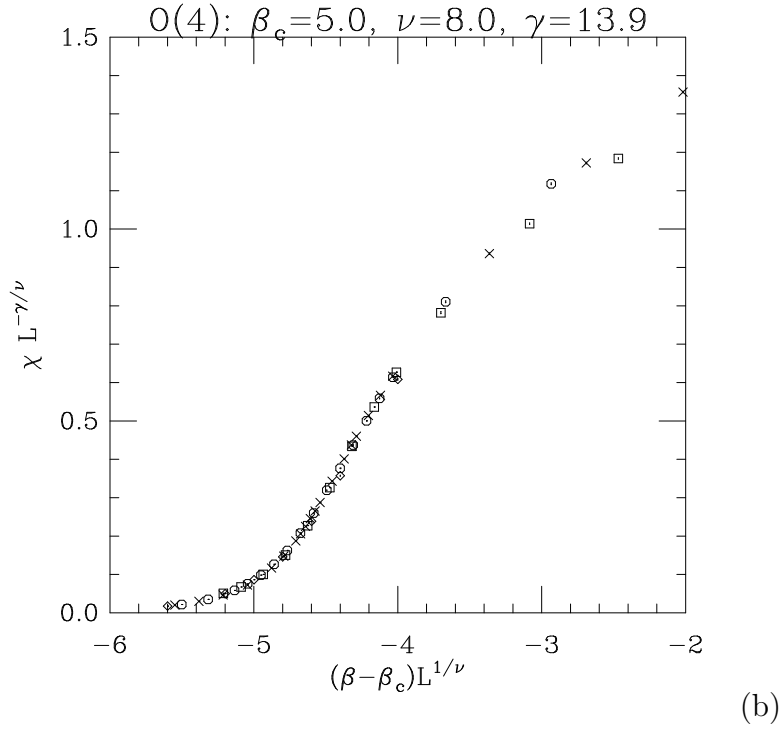
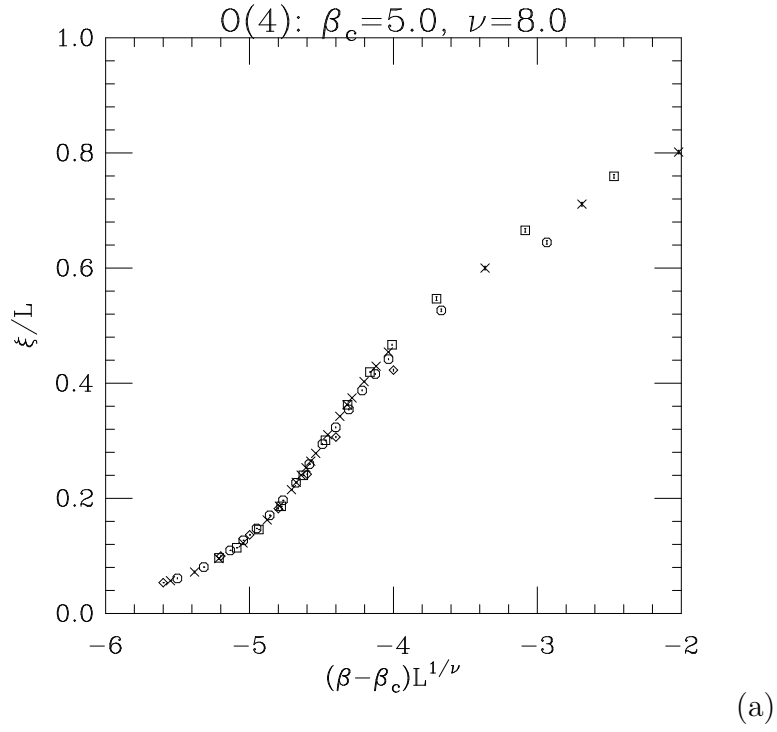


Figure 9: Finite-size-scaling plot of ξ/L (a) and $\chi L^{-\gamma/\nu}$ (b) versus $(\beta - \beta_c)L^{1/\nu}$, for lattice sizes $L = 32$ (\square), 64 (\times), 128 (\circ), 256 (\diamond). Here $\beta_c = 5.0$, $\nu = 8.0$ and $\gamma = 13.9$. Error bars are in most cases invisible.

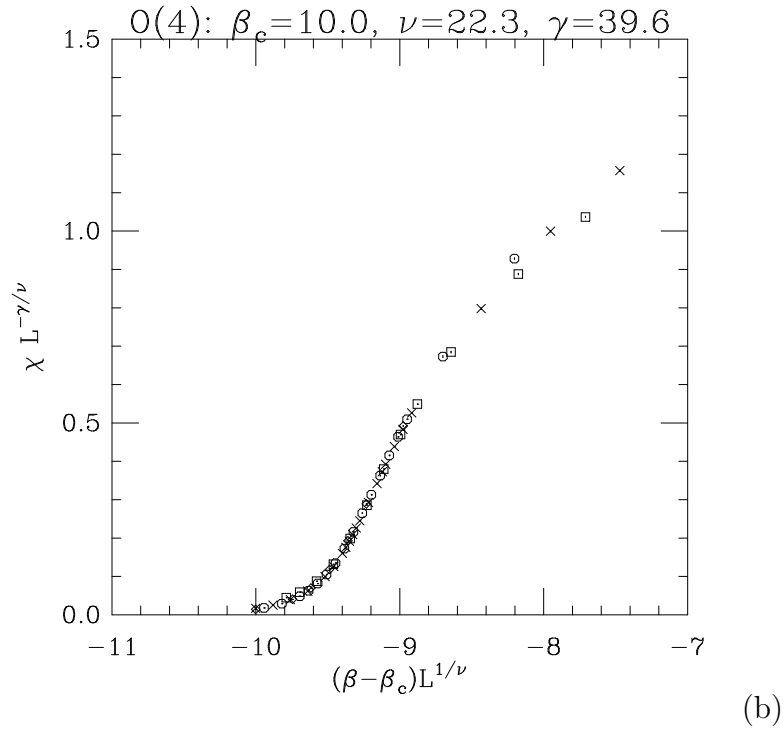
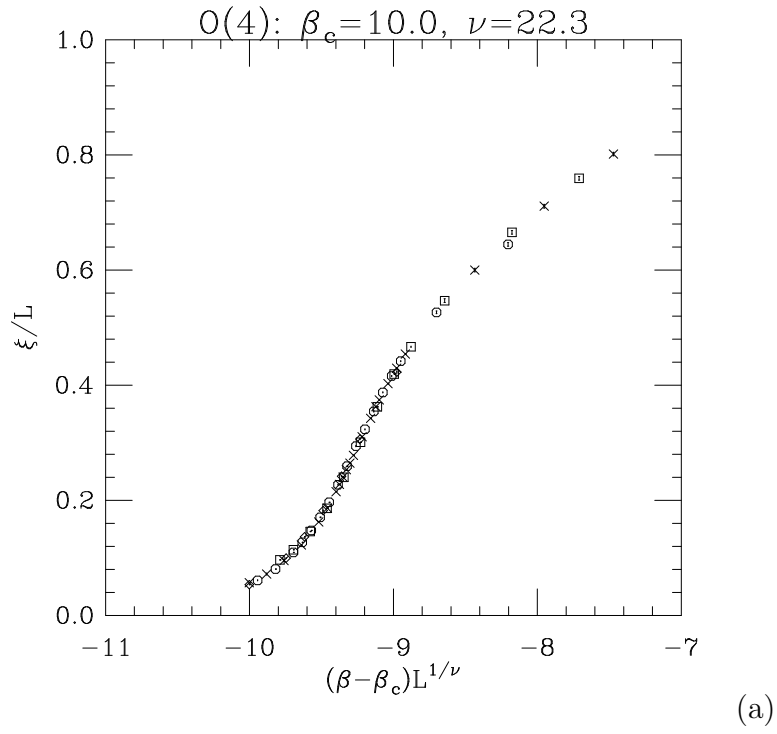


Figure 10: Finite-size-scaling plot of ξ/L (a) and $\chi L^{-\gamma/\nu}$ (b) versus $(\beta - \beta_c)L^{1/\nu}$, for lattice sizes $L = 32$ (\square), 64 (\times), 128 (\circ), 256 (\diamond). Here $\beta_c = 10.0$, $\nu = 22.3$ and $\gamma = 39.6$. Error bars are in most cases invisible.

(subjective 68% confidence limits). In Figures 11–14 we show the “best” finite-size-scaling plots for each case. Note that the corrections to scaling are quite strong: the $L = 32$ points deviate considerably from the asymptotic scaling curve, and even for $L = 64$ the deviation is noticeable (see Figures 12 and 13). However, it is reasonable to hope that these corrections to scaling will have decayed to a small value by $L = 128$; if so, our estimates of z_{int, \mathcal{M}^2} for the V- and W-cycles — which attempt to place the $L = 128$ and $L = 256$ points on top of one another — will be afflicted by only a small systematic error. In any case, the error bars in (3.28) take account of this potential systematic error.

Note also that the finite-size effects on dynamic quantities are *extremely strong*, even at $\xi/L \lesssim 0.2$ where the finite-size effects on static quantities are very weak: compare Figures 11–14 with Figures 2–3. Indeed, in the heat-bath case (Figure 11) it is far from clear that $g_{\mathcal{M}^2}(0) = \lim_{x \downarrow 0} g_{\mathcal{M}^2}(x)$ is finite as it should be; additional data at smaller values of ξ/L would be needed to verify this. In the W-cycle case it does seem likely that $g_{\mathcal{M}^2}(0)$ is finite and nonzero ($\approx 0.3?$); but the scaling function $g_{\mathcal{M}^2}(x)$ may well vary by as much as a factor of 2 in the range $x \equiv \xi/L \lesssim 0.1$. We conclude that finite-size corrections to dynamic critical behavior can be surprisingly strong; therefore, serious studies of dynamic critical phenomena *must* include a finite-size-scaling analysis. It can be very misleading to assume that the finite-size corrections to dynamic quantities are small simply because ξ/L is small, or because the finite-size corrections to *static* quantities are small.

Applying the same procedure to $\tau_{int, \vec{\mathcal{M}}}$, we obtain

$$z_{int, \vec{\mathcal{M}}} = \begin{cases} 2.0 \pm 0.20 & \text{for the heat-bath} \\ 1.22 \pm 0.09 & \text{for the V-cycle} \end{cases} \quad (3.29)$$

(subjective 68% confidence limits). In Figures 15 and 16 we show the “best” finite-size-scaling plots for each case. For this observable the finite-size corrections are much weaker.

3.5 Computational Work

In Table 7, we show the CPU time per iteration for our MGMC program running on one processor of a Cray Y-MP 8/832, as a function of $L = 32, 64, 128, 256$ and $\gamma = 0, 1, 2, 3$. The data deviate from the predicted behavior (2.9) for two reasons: Firstly, the fine-grid Hamiltonian (2.1) is simpler than the coarse-grid Hamiltonians (2.5), and we have exploited this by writing special streamlined versions of the heat-bath and “compute H_{l-1} ” subroutines for the finest grid alone. Therefore, the CPU time on each grid other than the finest is a factor $C \approx 2$ greater than the estimate (2.9) assumes. Secondly, the vectorization is more effective on the larger lattices because the vectors are longer, so the CPU time grows less than proportionately to the volume, at least through $L = 256$.

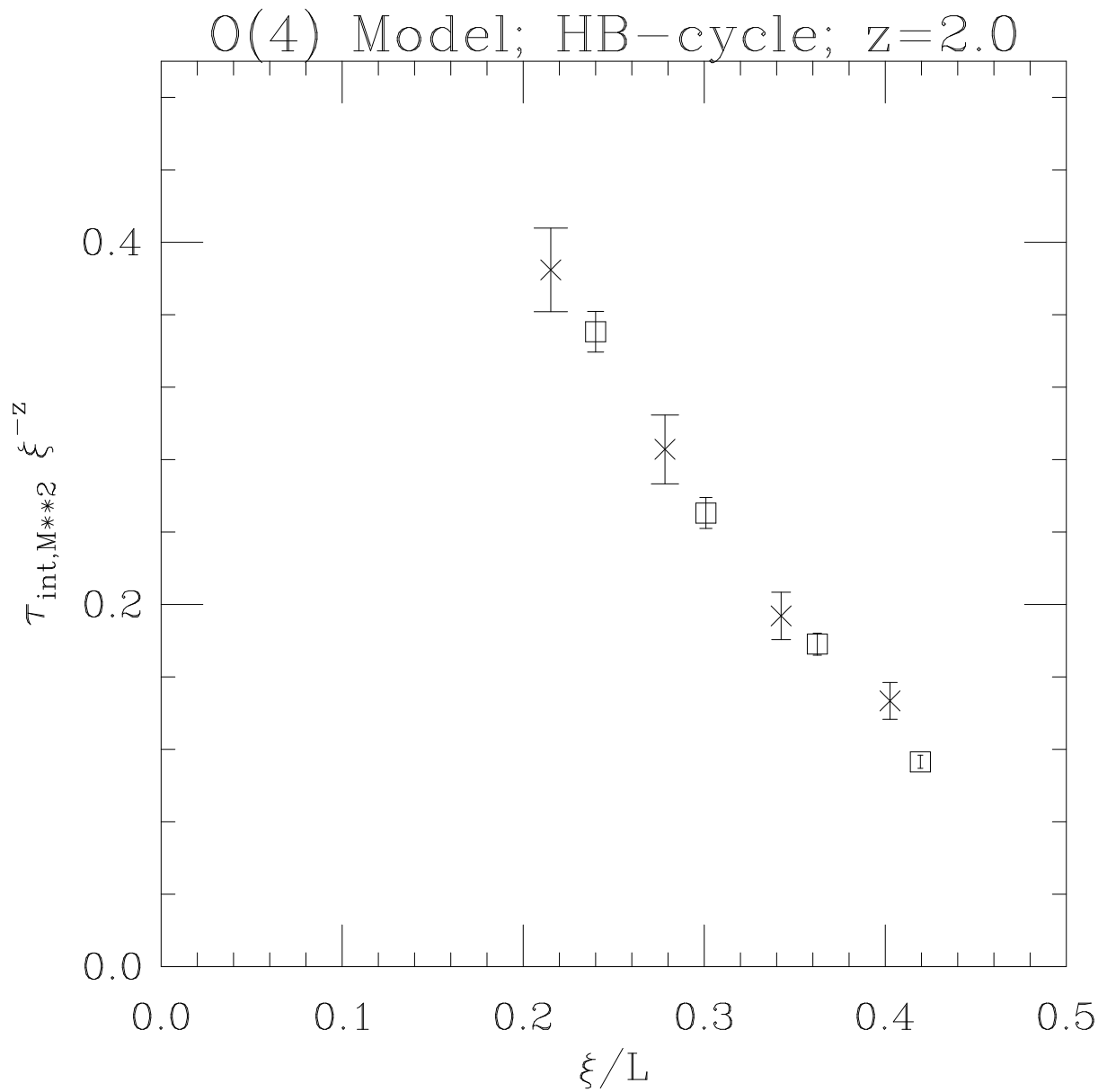


Figure 11: Finite-size-scaling plot of $\tau_{int, \mathcal{M}^2} \xi^{-z_{int, \mathcal{M}^2}}$ versus ξ/L for the heat-bath algorithm, for lattice sizes $L = 32$ (\square) and 64 (\times). Here $z_{int, \mathcal{M}^2} = 2.0$.

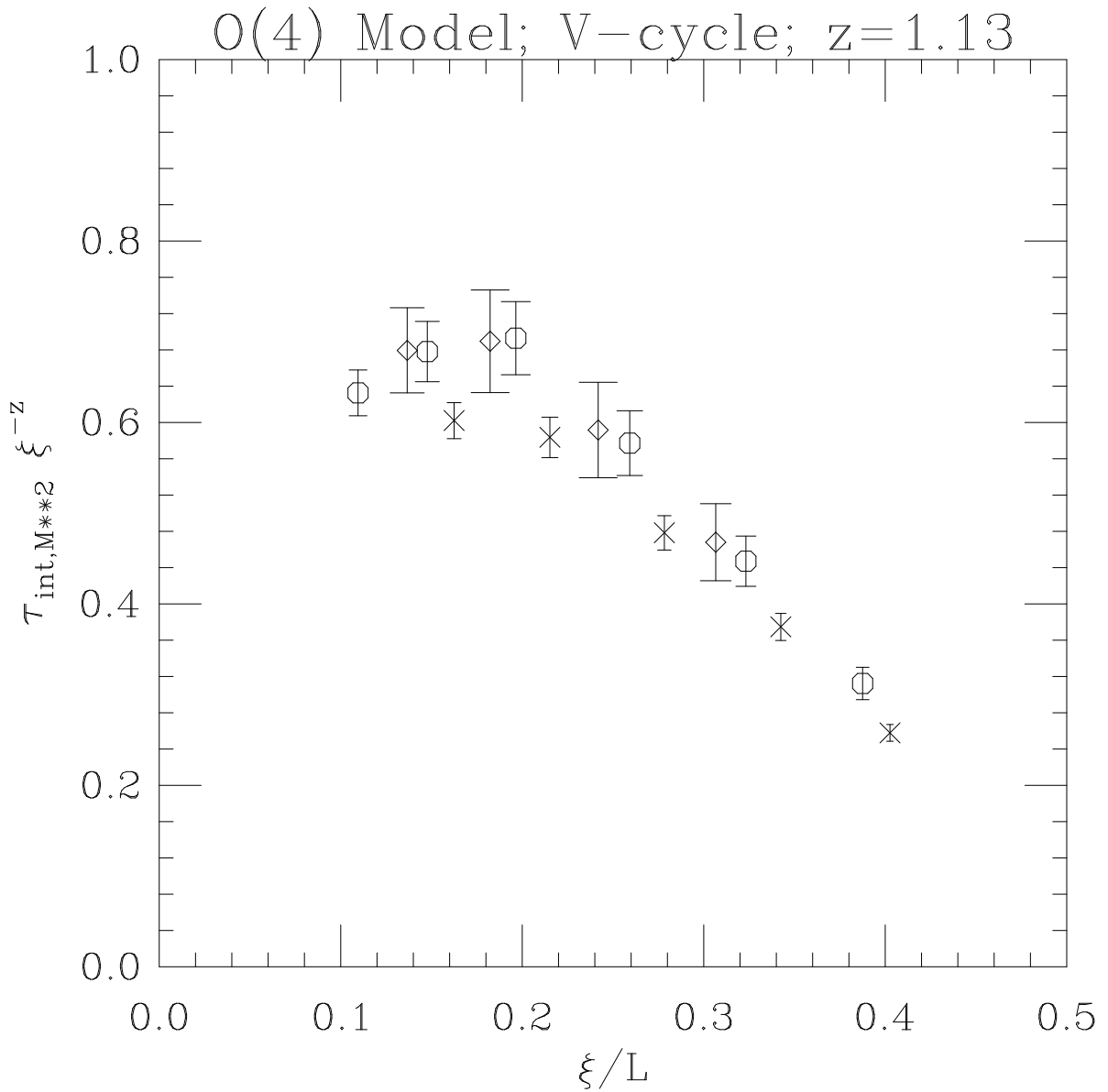


Figure 12: Finite-size-scaling plot of $\tau_{int, M^2} \xi^{-z_{int, M^2}}$ versus ξ/L for the V-cycle algorithm, for lattice sizes $L = 64$ (\times), 128 (\circ) and 256 (\diamond). Here $z_{int, M^2} = 1.13$.

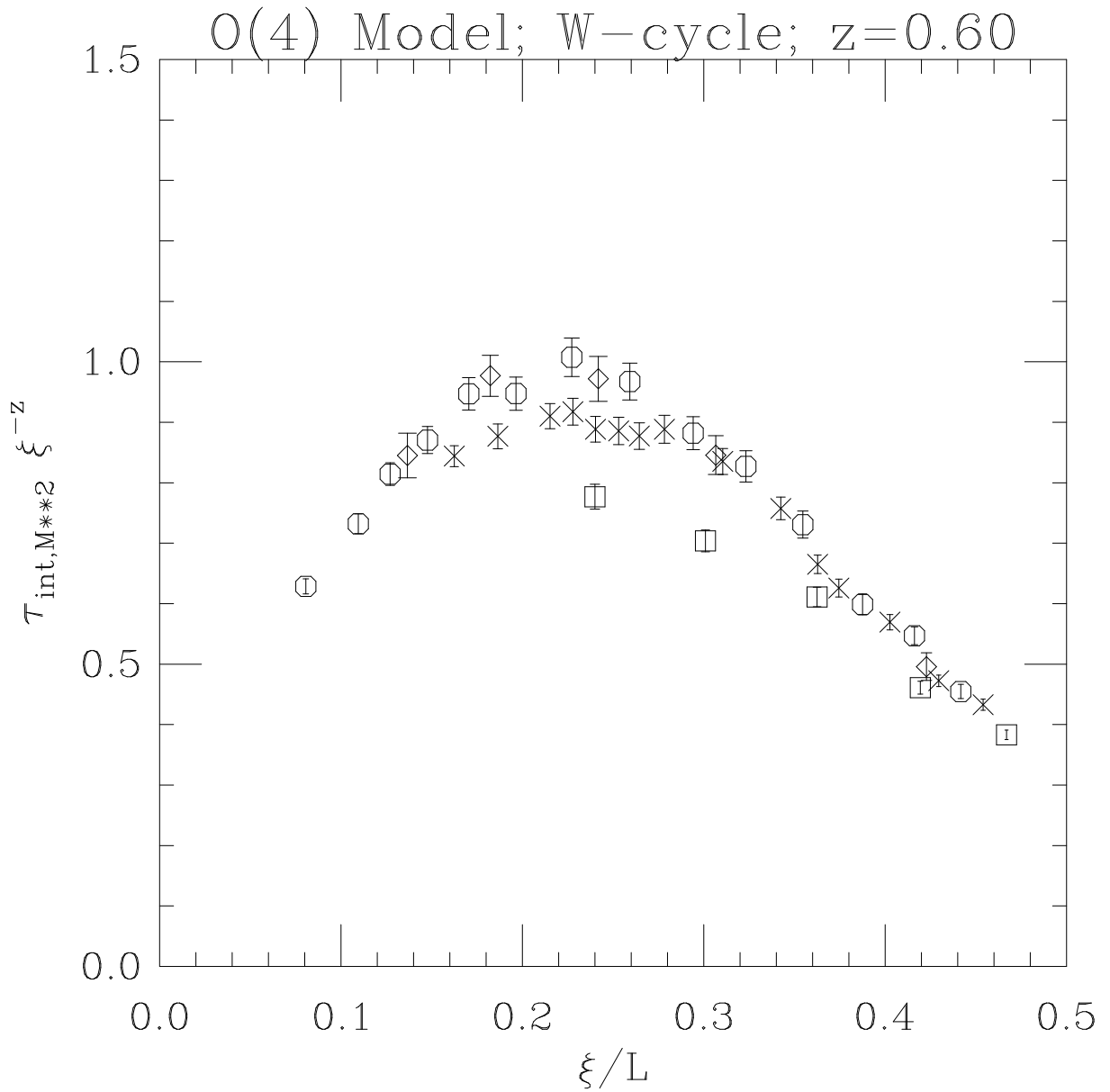


Figure 13: Finite-size-scaling plot of $\tau_{int, \mathcal{M}^2} \xi^{-z_{int, \mathcal{M}^2}}$ versus ξ/L for the W-cycle algorithm, for lattice sizes $L = 32$ (\square), 64 (\times), 128 (\circ) and 256 (\diamond). Here $z_{int, \mathcal{M}^2} = 0.60$.

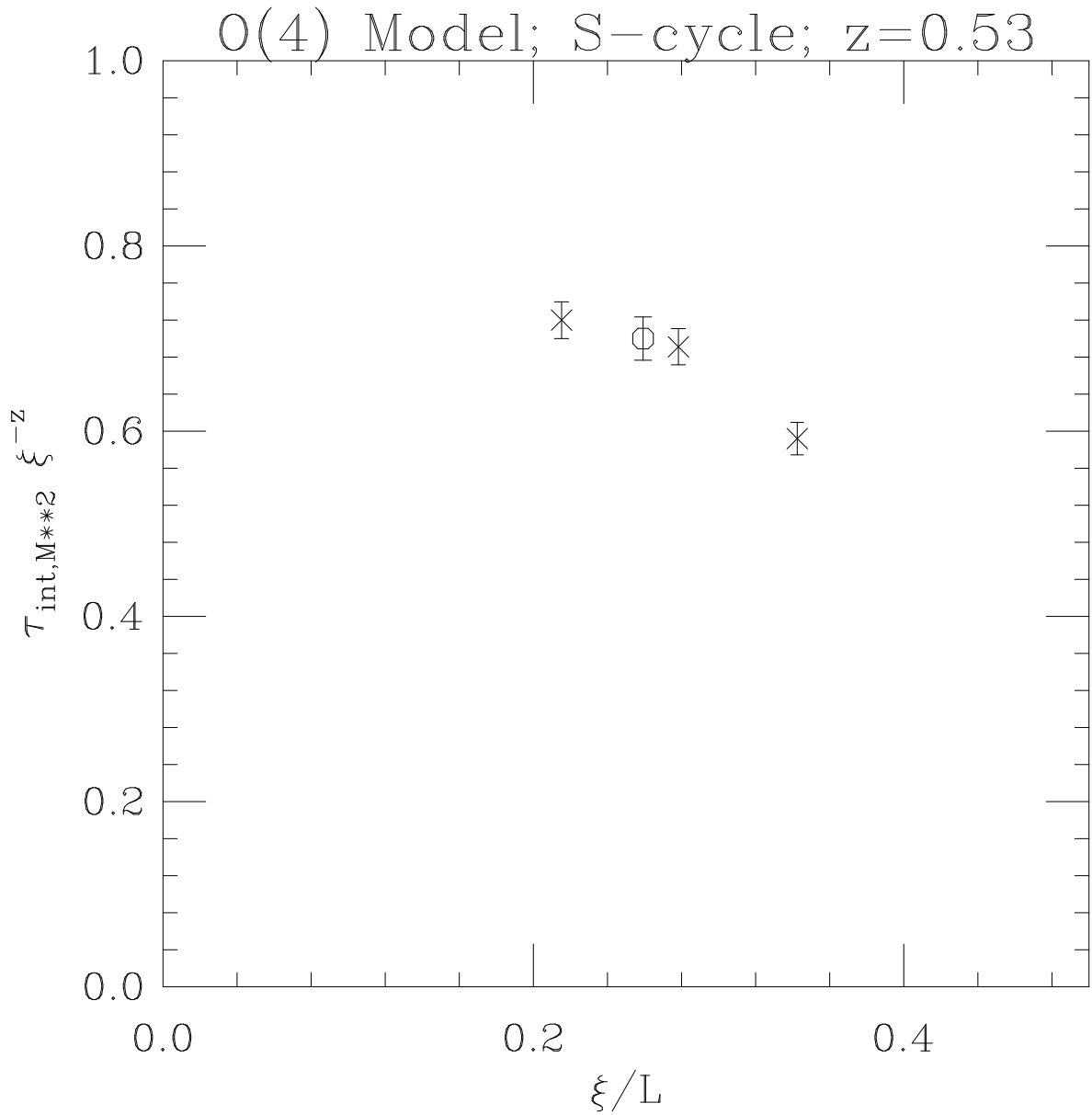


Figure 14: Finite-size-scaling plot of $\tau_{int, \mathcal{M}^2} \xi^{-z_{int, \mathcal{M}^2}}$ versus ξ/L for the super-W-cycle algorithm, for lattice sizes $L = 64$ (\times) and 128 (\circ). Here $z_{int, \mathcal{M}^2} = 0.53$.

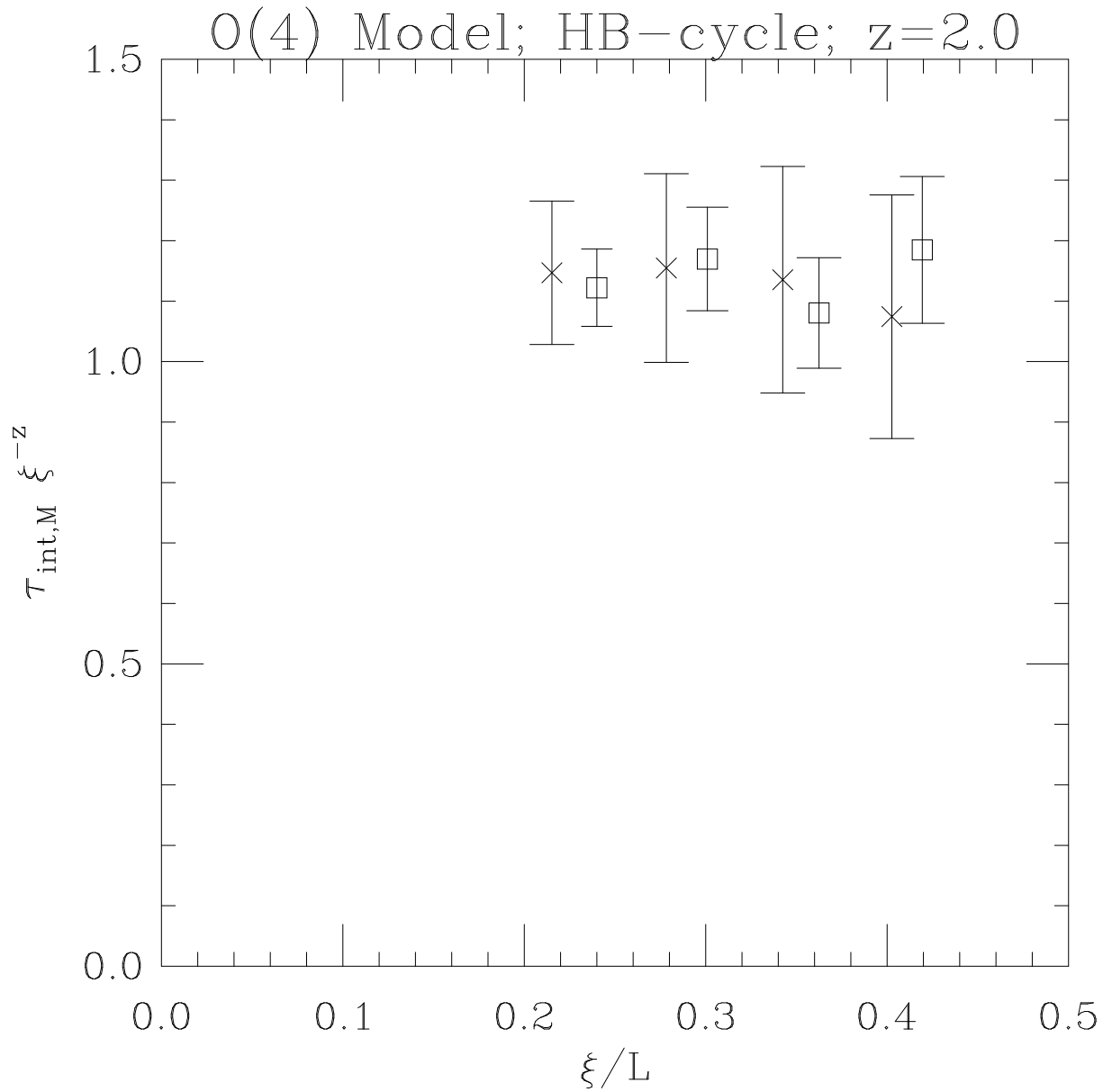


Figure 15: Finite-size-scaling plot of $\tau_{int,\bar{\mathcal{M}}}\xi^{-z_{int,\bar{\mathcal{M}}}}$ versus ξ/L for the heat-bath algorithm, for lattice sizes $L = 32$ (\square) and 64 (\times). Here $z_{int,\bar{\mathcal{M}}} = 2.0$.

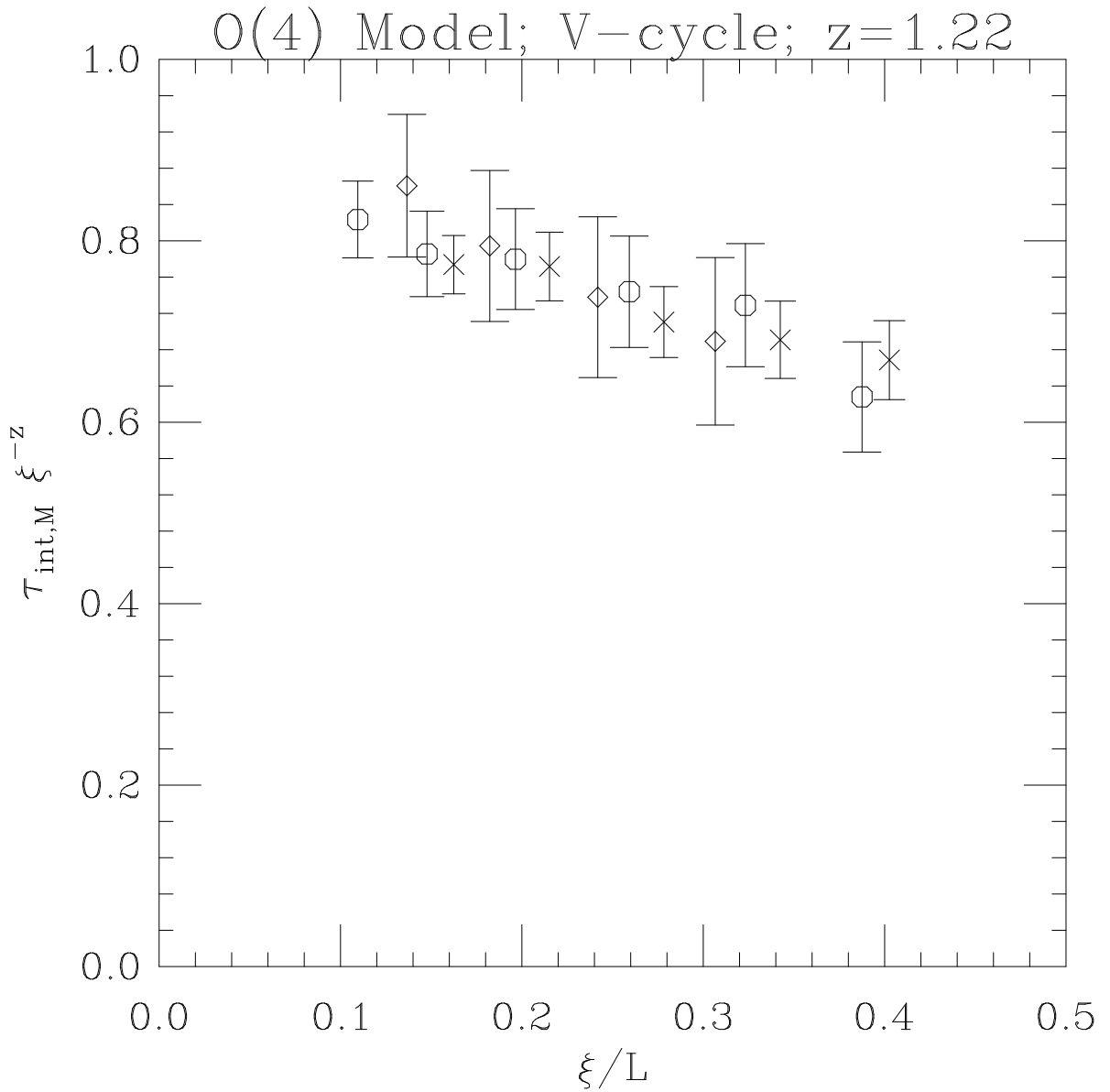


Figure 16: Finite-size-scaling plot of $\tau_{int,\mathcal{M}} \xi^{-z_{int,\mathcal{M}}}$ versus ξ/L for the V-cycle algorithm, for lattice sizes $L = 64$ (\times), 128 (\circ) and 256 (\diamond). Here $z_{int,\mathcal{M}} = 1.22$.

CPU timings for $O(4)$ MGMC				
L	$\gamma = 0$	$\gamma = 1$	$\gamma = 2$	$\gamma = 3$
32	5.9	12.2	33.0	92.4
64	18.7	33.8	88.9	301.2
128	66.3	109.6	256.7	986.2
256	252.8	397.6	815.3	3305.2

Table 7: CPU times in milliseconds per iteration for MGMC algorithm for the two-dimensional $O(4)$ model with $m_1 = m_2 = 1$ and $\gamma = 0, 1, 2, 3$, on a Cray Y-MP 8/832.

The running speed for our program at $L = 256$ was about 100 MFlops. The total CPU time for the runs reported here was about 650 hours.

The statistical efficiency of a Monte Carlo algorithm is inversely proportional to the integrated autocorrelation time for the observable(s) of interest, *measured in CPU units*. For the W-cycle at $L = 256$, $\beta = 2.6$ (corresponding to $\xi \approx 47$), we have $\tau_{int, \mathcal{M}^2} \approx 8$ Cray seconds for a W-cycle, compared to ≈ 43 seconds for a V-cycle, and ≈ 280 seconds for a heat bath. (The heat-bath value is an extrapolation from the $L = 64$, $\beta = 2.2$ point, using finite-size-scaling together with our result $z_{int, \mathcal{M}^2, HB} \approx 2$.) Thus, on a 256×256 lattice the W-cycle MGMC algorithm is about 35 times as efficient as a heat-bath algorithm.

4 Discussion

4.1 Heuristic Predictions for z

In paper I [6, Section IX.C] we predicted that for an asymptotically free theory with a continuous symmetry group, such as the $O(N)$ σ -model ($N > 2$), the MGMC algorithm using piecewise-constant interpolation and a W-cycle would completely eliminate critical slowing-down except for a possible logarithm. Our data in Section 3.4 show clearly that this prediction is *incorrect*: the exponent $z_{W-cycle} = 0.60 \pm 0.07$ is manifestly *not* equal to zero. It is obviously of great importance to understand heuristically what is going on here.

Our argument in [6] went as follows: For an asymptotically free theory with a continuous symmetry group, the important excitations at short wavelengths are weakly-interacting spin waves, i.e. the theory at short wavelengths is *almost Gaussian*. Now, we know [63] that MGMC with piecewise-constant interpolation and a W-cycle *completely eliminates* critical slowing-down in a Gaussian model. Therefore, we expect that MGMC will *almost* perfectly handle the short-wavelength modes of an asymptotically free theory. On the other hand, we know that the long-wavelength modes of an asymptotically free theory are strongly non-Gaussian (e.g. there is strong scattering [14]), and we do not expect MGMC to handle these modes well. Suppose, therefore, that the modes of wavelength $\lesssim \ell_{max}$ are well handled by MGMC moves on the corresponding grids (in the sense that the autocorrelation time for these modes is of order 1), but that coarse-grid moves on scales $\gtrsim \ell_{max}$ are ineffective. In this case, the correlation length “seen” on the grid of scale ℓ_{max} will be of order ξ/ℓ_{max} ; and since further coarse grids are ineffective, we expect the autocorrelation time of the MGMC

algorithm to be of order $\tau_{MGMC} \sim (\xi/\ell_{max})^{z_{HB}}$, where z_{HB} is the dynamic critical exponent of the single-site heat-bath algorithm.

The question is: *how big is ℓ_{max} ?* In [6] we assumed that $\ell_{max} \sim \xi$ (for example, $\ell_{max} \approx \xi/10$) or at worst $\ell_{max} \sim \xi/\log^p \xi$ — in which case we would have $\tau_{MGMC} \sim 1$ or $\tau_{MGMC} \sim \log^q \xi$, respectively. But this argument is, in retrospect, much too sloppy. An asymptotically free theory is indeed “almost” Gaussian at short length scales, but this Gaussianness is approached *very slowly*: on scale ℓ , the coupling strength (defined e.g. by the truncated 4-point function at momentum $p \sim 1/\ell$) behaves like $g(\ell) \sim 1/\log(\xi/\ell)$. Now, suppose that this non-Gaussianness causes MGMC to make small “mistakes”¹⁶; and suppose that these “mistakes” accumulate (additively) over successive length scales until they reach order 1, at which point MGMC becomes ineffective. The length scales (i.e. grids) are indexed by $\log_2 \ell$. This hand-waving argument suggests that ℓ_{max} should be given by the relation

$$\int_1^{\ell_{max}} \frac{1}{\log(\xi/\ell)} d(\log \ell) \approx C, \quad (4.1)$$

where C is a constant of order 1. It follows that

$$\ell_{max} \sim \xi^p, \quad (4.2)$$

where

$$p = 1 - e^{-C} \quad (4.3)$$

lies strictly between 0 and 1 (but we are unable to say more than this). Hence we predict that $z_{MGMC} = pz_{HB}$ lies strictly between 0 and z_{HB} — a very weak prediction, but one that seems at least to be true.

(We remark that this heuristic argument is very unstable to small perturbations. Suppose, for example, that we take instead $g(\ell) \sim 1/\log^p(\xi/\ell)$ with some exponent $p \neq 1$. Then if $p < 1$ we get $\ell_{max} \sim O(1)$, while if $p > 1$ we get $\ell_{max} \sim \xi$. So $p = 1$ is a very delicate borderline case. Thus, our heuristic argument, if in fact it is correct, depends crucially on the particular measure of “non-Gaussianness” that we have chosen.)

On the other hand, for the V-cycle the observed exponents $z_{int, \mathcal{M}^2, V-cycle} = 1.13 \pm 0.11$ and $z_{int, \vec{\mathcal{M}}, V-cycle} = 1.22 \pm 0.09$ are very close to the believed behavior $z_{V-cycle} = 1$ of the Gaussian model [see the discussion following (2.10)]. This suggests that in V-cycle MGMC (with piecewise-constant interpolation) for an asymptotically free model, the slowest modes are indeed the Gaussian-like long-wavelength spin waves. It would be interesting to know whether $z_{V-cycle}$ for the $O(4)$ model is exactly equal to 1 (possibly modulo a logarithm), or is slightly higher as our data suggest.

¹⁶ By “mistakes” we do *not* mean to imply a failure to simulate the correct Gibbs measure; of course, by construction, the unique invariant measure of the MGMC algorithm is the correct Gibbs measure. Rather, we mean a failure to generate *independent* samples from this Gibbs measure in a time of order 1.

4.2 Piecewise-Constant vs. Smooth Interpolation

As noted at the end of Section 2, Mack and collaborators [67, 68, 47, 69] have advocated the use of a smooth interpolation (e.g. piecewise-linear or better) in place of piecewise-constant. The key question is this: Does the MGMC algorithm have a *different dynamic critical exponent* depending on whether smooth or piecewise-constant interpolation is used?

In the Gaussian case, the answer is “yes” for a V-cycle but “no” for a W-cycle, as discussed in Section 2. For non-Gaussian asymptotically free models, we conjecture that the answer is the same, but to date no full-scale test has been made. Hasenbusch, Meyer and Mack [47] have reported preliminary data for the $O(3)$ model suggesting that $z_{int,\mathcal{M}^2} \approx 1.2$ for a V-cycle with piecewise-constant interpolation, compared to $z_{int,\mathcal{M}^2} \approx 0.2$ for a V-cycle with smooth interpolation. (These authors have not studied a W-cycle, as this would be extremely costly in their “unigrid” approach, but it is safe to assume that $z_{W-cycle} \leq z_{V-cycle}$.) For the piecewise-constant V-cycle, this estimate is very close to ours. But the estimate for the smooth-interpolation V-cycle (and hence also the smooth-interpolation W-cycle) is considerably lower than our estimate $z_{int,\mathcal{M}^2} \approx 0.6$ for the piecewise-constant W-cycle — suggesting that the smooth interpolation might indeed lead to a smaller dynamic critical exponent than piecewise-constant interpolation, even for a W-cycle. However, this estimate is based on runs at only four (β, L) pairs, which moreover have different values of ξ_∞/L , so it is very difficult to perform a correct finite-size-scaling analysis. It would be very useful to have data at additional (β, L) pairs, and with higher statistics.

It should also be noted that since the dynamic critical exponent for MGMC in asymptotically free models is apparently nontrivial (i.e. $z \neq 0, 1, 2$), it is reasonable to expect this exponent to be *different* for each asymptotically free model: for example, in the $O(N)$ models the exponent would depend on N — albeit probably weakly — just as static exponents in nontrivial N -vector models (such as those in $d = 3$) depend on N . For this reason, it would be very useful to have data comparing the two interpolations at the *same* value of N .

A very recent preprint by Hasenbusch and Meyer [69] gives preliminary data for the $SU(3)$ and CP^3 σ -models in two dimensions, using a V-cycle with piecewise-linear interpolation. For CP^3 the data are consistent with the dynamic finite-size-scaling Ansatz (3.27) with $z_{int,\mathcal{M}^2} \approx 0.3 \pm 0.1$. For $SU(3)$, however, the data are very erratic, and do not appear to be consistent with (3.27). More data would be very useful here too.

4.3 Comparison with Other Collective-Mode Algorithms

It is of great interest to compare the behavior of MGMC with that of Fourier acceleration [74, 75, 76, 77]. The two algorithms are very similar in spirit: both are motivated by the Gaussian model (for which they eliminate critical slowing-down entirely); both make additive updates of a fixed-shape collective mode. The principal difference is the choice of this collective mode: for Fourier acceleration it is a sine wave, while for MGMC it is a square wave (or triangular wave if one uses piecewise-linear interpolation). Of course, the “correct” collective modes in the Gaussian model are sine waves; but the MGMC convergence proof [63] shows that square waves are “close enough” (for a W-cycle). There is one additional difference: Fourier acceleration is based on small-amplitude updates (i.e. a Langevin or hybrid algorithm), while MGMC is based on arbitrary-amplitude updates (a heat-bath algorithm).

These close analogies between MGMC and Fourier acceleration suggest that their behavior may be qualitatively similar, in the sense that they work well for the same models and work badly for the same models. More precisely, we expect that on length scales where the dominant collective modes are very weakly interacting spin waves, both MGMC and Fourier acceleration will handle such modes well. On the other hand, on length scales where the dominant collective modes are strongly non-Gaussian — either because the spin waves are strongly interacting, as in the σ -model at $\ell \gtrsim \ell_{max}$, or because these modes are inherently discrete, as in the one-component φ^4 model or the high-temperature phase of the two-dimensional XY model — we expect that *neither* MGMC nor Fourier acceleration will work particularly well: they will gain either a constant factor in efficiency over the local algorithms, or perhaps a small reduction in the dynamic critical exponent. (For some nonlinear models, Fourier acceleration might work significantly worse than MGMC, if barrier penetration by the small-amplitude updates becomes a limiting factor. This difficulty is unrelated to *critical* slowing-down; for example, it occurs already for the double-well φ^4 model with *one* lattice site.)

To test this hypothesis, we would like to compare the dynamic critical behavior of MGMC and Fourier acceleration for the σ -model. Unfortunately, there is at present very little published data on the dynamic critical behavior of Fourier acceleration. Studies of the two-dimensional XY model [75, 76] were discussed in paper II [7]. The only other published test of Fourier acceleration of which we are aware is a study of the two-dimensional $SU(3)$ principal chiral model by Dagotto and Kogut [77]. This article reported $\tau_{int, \mathcal{M}^2}$ and $\tau_{int, \mathcal{E}}$ for Langevin and hybrid algorithms with and without Fourier acceleration, on lattices of size 16^2 and 32^2 , for several temperatures in the scaling region. The results indicate qualitatively that $z \ll 2$ for the hybrid algorithm with Fourier acceleration, but the data are unfortunately too crude to allow quantitative conclusions to be drawn.

The available data are in any case at least roughly consistent with the conjecture that, for each model, Fourier acceleration and MGMC have qualitatively similar, and possibly even identical, dynamic critical exponents. However, it would be desirable to have more precise and comprehensive measurements of the dynamic critical behavior of the Fourier-accelerated Langevin and hybrid algorithms, so as to test this conjecture of dynamic (quasi-)universality.¹⁷ It would also be desirable to have precise measurements of the dynamic critical exponent of MGMC for another asymptotically free model, such as the $SU(3)$ principal chiral model, in order to determine whether z varies from one such model to another.

A very different type of collective-mode algorithm for N -vector models was proposed very recently by Wolff [41], and independently by Hasenbusch [43]. This algorithm is based on embedding a field of Ising variables into the N -vector model, and then simulating the induced Ising model by the Swendsen-Wang [80] algorithm (or a variant thereof [41]). It can be argued heuristically [42] that this algorithm is effective at creating long-wavelength spin waves, and extensive numerical tests show that critical slowing-down is entirely (or almost

¹⁷ We emphasize that a fair test must use the *exact* versions of the Langevin [78] and hybrid [79] algorithms, and should tune the step-size in these algorithms (separately for each β and L) so as to optimize the autocorrelation time. We emphasize also that Fourier acceleration most likely encompasses a *continuously infinite family* of dynamic universality classes, according to the long-distance (low-momentum) properties of the acceleration kernel.

entirely) eliminated in the two-dimensional N -vector models for $N = 2, 3, 4$ [41, 42, 44, 49].¹⁸

The principal difference between MGMC and Fourier acceleration on the one hand, and algorithms of Swendsen-Wang and Wolff type on the other, is how proposals are made for updating the long-wavelength modes. MGMC and Fourier acceleration propose additive updates of *fixed* shape (sinusoidal, triangular or square) and variable amplitude, while cluster algorithms like Swendsen-Wang and Wolff allow the system, in some sense, to *choose its own collective modes*.

At present, the Wolff-Swendsen-Wang algorithm is clearly the best algorithm for simulating N -vector models (at least in an unbroken phase): it is as efficient as MGMC for the two-dimensional XY model in the spin-wave regime, it is somewhat more efficient for two-dimensional asymptotically free σ -models, and it is far more efficient for the two-dimensional XY model in the vortex regime — and it is much simpler to program. On the other hand, the MGMC algorithm has a natural extension to σ -models taking values in an arbitrary homogeneous space G/H , and at least in principle to lattice gauge theories [6, Sections IV and V]; but it is as yet far from clear whether an efficient Wolff-type embedding algorithm can be devised for these models. Indeed, in a separate work [49] we argue that the generalized Wolff-type embedding algorithm can have dynamic critical exponent $z \ll 2$ *only* if the target manifold is a sphere (as in the N -vector model), a product of spheres, or the quotient of such a space by a discrete group (e.g. real projective space RP^{N-1}). Finally, Fourier acceleration applies to all continuous-spin models, even in the presence of dynamical fermions (which is its greatest advantage); but the restriction to small step size is a disadvantage, and the need to optimize several tunable parameters makes it more complicated to test and to use. We therefore believe that all three classes of collective-mode algorithms — Fourier acceleration, MGMC and embedding algorithms — should be developed in parallel, in order to determine the conditions under which each one works well or badly. In particular, we advocate that a standard test procedure be developed (which autocorrelation times to measure, what statistical procedures to use) so that test results obtained by diverse research groups can be readily compared.

Acknowledgments

We want to thank Achi Brandt, Richard Brower, Martin Hasenbusch, Steffen Meyer, Claudio Parrinello and Ulli Wolff for several helpful suggestions. The computations reported here were carried out on the Cray Y-MP at the Pittsburgh Supercomputing Center (PSC). This work was supported in part by the U.S. National Science Foundation grants DMS-8705599 and DMS-8911273 (J.G. and A.D.S.), by the U.S. Department of Energy through contracts DE-FC05-85ER250000 (R.G.E.) and DE-FG02-90ER40581 (A.D.S.), and by PSC grant PHY890025P. One of the authors (S.J.F.) was supported by the Conselho Nacional de Pesquisas (Brazil), and another of the authors (J.G.) was partially supported by a Sloan Foundation Fellowship.

¹⁸ For $N = 2$ this requires that the algorithm also be effective at creating vortex-antivortex pairs; the mechanism for this is explained in [42].

A Heat-Bath Algorithm for the N -Vector Model

In implementing the heat-bath step of the MGMC algorithm for the $SU(2)$ principal chiral model, we need a subroutine that generates a random matrix $U \in SU(2)$ from the probability distribution

$$d\mu(U) = \text{const} \times \exp(\text{tr} M^\dagger U) dU , \quad (\text{A.1})$$

where M is a fixed matrix lying in the linear span of $SU(2)$, and dU is Haar measure. Since $M = \lambda V$ with $\lambda = (\det M)^{1/2} \geq 0$ and $V \in SU(2)$, and U can be parametrized in the form (1.2), it clearly suffices to generate a random unit vector $\boldsymbol{\sigma} = (\sigma^0, \sigma^1, \sigma^2, \sigma^3) \in \mathbb{R}^4$ from the probability distribution

$$d\nu(\boldsymbol{\sigma}) = \text{const} \times \exp(h\sigma^0) d\boldsymbol{\sigma} , \quad (\text{A.2})$$

where $d\boldsymbol{\sigma}$ is uniform measure on the unit sphere in \mathbb{R}^4 (here $h = 2\lambda$). More generally, we can pose this latter problem for unit vectors in \mathbb{R}^N ($N \geq 2$); this problem arises also in implementing the heat-bath algorithm for an N -vector model. The problem then divides naturally into two parts:

- (a) Generate the component $t \equiv \sigma^0$ with probability density proportional to

$$f(t) = e^{ht} (1 - t^2)^{(N-3)/2} dt \quad (\text{A.3})$$

restricted to the interval $[-1, 1]$. We can assume without loss of generality that $h \geq 0$.

- (b) Generate $\boldsymbol{\sigma}^\perp \equiv (\sigma^1, \dots, \sigma^{N-1})$ to be a random vector on the sphere of radius $(1 - t^2)^{1/2}$ in \mathbb{R}^{N-1} .

The principal purpose of this Appendix is to discuss three methods for solving problem (a).¹⁹ At the end we shall make some brief remarks about the much easier problem (b).

All of our methods are based on the von Neumann rejection technique [83, 82]: given a function $g(t) \geq f(t)$, we generate a random variable T with density proportional to $g(t)$ and then accept it with probability $f(T)/g(T)$; we keep trying until success. The acceptance probability is

$$A = \frac{\int_{-\infty}^{\infty} f(t) dt}{\int_{-\infty}^{\infty} g(t) dt} , \quad (\text{A.4})$$

and the expected number of trials is A^{-1} . Obviously, g must be simple enough that we can conveniently generate a random variable with density proportional to g ; but subject to this constraint we want g to be as similar to f as possible. Our three methods are based on different choices of the trial distribution g :

Method 1 (valid only for $N \geq 3$). $g(t) = e^{ht}$ restricted to $[-1, 1]$. Such a random variable can be generated by transformation:

$$T = h^{-1} \log[e^{-h} + (e^h - e^{-h})U] , \quad (\text{A.5})$$

¹⁹ For the special case $N = 2$, one additional method (rejection from a Gaussian in the angular variables) was discussed in the Appendix of [7], and several different methods are discussed in [81]. See also [82, pp. 473–476].

where U is uniform on $[0, 1]$. The proposal is accepted with probability $(1 - t^2)^{(N-3)/2}$. The acceptance probability is

$$A = 2^{(N-2)/2} \sqrt{\pi} \Gamma\left(\frac{N-1}{2}\right) h^{2-(N/2)} (e^h - e^{-h})^{-1} I_{(N-2)/2}(h) \quad (\text{A.6})$$

$$= \begin{cases} \frac{\sqrt{\pi} \Gamma(\frac{N-1}{2})}{2\Gamma(\frac{N}{2})} \left[1 - \frac{N-3}{6N} h^2 + O(h^4)\right] & \text{as } h \rightarrow 0 \\ 2^{(N-3)/2} \Gamma\left(\frac{N-1}{2}\right) h^{-(N-3)/2} \left[1 + O(h^{-1})\right] & \text{as } h \rightarrow \infty \end{cases} \quad (\text{A.7})$$

By construction this algorithm works perfectly for $N = 3$. For $N > 3$ it works decently but not perfectly for small h (and deteriorates there when N is very large), and badly at large h . For the case $N = 4$, this method was proposed previously by Creutz [84].

Method 2 (valid only for $N \geq 3$). $g(t) = e^{ht}[2(1-t)]^{(N-3)/2}$ restricted to $(-\infty, 1]$. This is expressed more conveniently by making the change of variables $s = 1 - t$. Then the desired distribution is

$$\tilde{f}(s) = e^{-hs} s^{(N-3)/2} (2-s)^{(N-3)/2} \quad (\text{A.8})$$

restricted to $[0, 2]$, the trial distribution is

$$\tilde{g}(s) = e^{-hs} (2s)^{(N-3)/2} \quad (\text{A.9})$$

on $[0, \infty)$, and the proposal is accepted with probability

$$\frac{\tilde{f}(s)}{\tilde{g}(s)} = \begin{cases} \left(1 - \frac{s}{2}\right)^{(N-3)/2} & \text{if } 0 \leq s \leq 2 \\ 0 & \text{if } s > 2 \end{cases} \quad (\text{A.10})$$

The trial S is a Gamma $\left(\frac{N-1}{2}, h^{-1}\right)$ random variable; for N a positive integer, such a random variable can be generated by combining exponential and Gaussian random variables [82, p. 405], and this algorithm is efficient if N is not too large. The acceptance probability is Method 2 is

$$A = (2\pi h)^{1/2} e^{-h} I_{(N-2)/2}(h) \quad (\text{A.11})$$

$$= \begin{cases} \frac{2\sqrt{\pi}}{\Gamma(N/2)} \left(\frac{h}{2}\right)^{(N-1)/2} \left[1 + O(h)\right] & \text{as } h \rightarrow 0 \\ 1 - \frac{(N-3)(N-1)}{8h} + O(h^{-2}) & \text{as } h \rightarrow \infty \end{cases} \quad (\text{A.12})$$

where I_ν is a modified Bessel function. Method 2 is extremely bad for small h (especially for large N), but it is quite efficient for large h . For the case $N = 4$, this method was proposed previously by several authors [85, 86, 87].

Method 3. $g(t) = e^h(1-t^2)^{(N-3)/2}$ restricted to $[-1, 1]$. This is a Beta $\left(\frac{N-1}{2}, \frac{N-1}{2}\right)$ distribution, which can be generated from a pair of Gamma $\left(\frac{N-1}{2}\right)$ variates or in many other ways [82, pp. 428–445]. The proposal is accepted with probability $e^{h(t-1)}$. The acceptance probability is

$$A = \Gamma\left(\frac{N}{2}\right) (h/2)^{-(N-2)/2} e^{-h} I_{(N-2)/2}(h) \quad (\text{A.13})$$

$$= \begin{cases} 1 - h + O(h^2) & \text{as } h \rightarrow 0 \\ 2^{(N-3)/2} \pi^{-1/2} \Gamma\left(\frac{N}{2}\right) h^{-(N-1)/2} \left[1 + O(h^{-1})\right] & \text{as } h \rightarrow \infty \end{cases} \quad (\text{A.14})$$

This works excellently for small h , and badly for large h . For the case $N = 2$, this method was studied in [7]: the trial variable T is produced by generating a uniform angle $\theta \in [0, 2\pi]$ and setting $T = \cos \theta$.

In Table 8 we show the acceptance probability as a function of h for each of the three methods, for the case $N = 4$. (However, the relevant issue in practice is not acceptance probability *per se*, but CPU time; the three methods have slightly different CPU time per trial.) Clearly it is necessary to use a combination of methods, in order to obtain a generator whose acceptance probability is bounded away from zero uniformly in h .²⁰ In our Monte Carlo studies of the $O(4)$ σ -model, we used Method 1 when $h \leq$ some h_{cutoff} , and Method 2 when $h > h_{cutoff}$. We vectorized the algorithm as follows: Gather all sites with $h \leq h_{cutoff}$, and compress them into a single vector; make one trial of Method 1; scatter the “successful” T values; gather and recompress the “failures”; and repeat until all sites are successful. Then do the same for sites with $h > h_{cutoff}$, using Method 2. Empirically we found that for runs in the physically interesting range of β values (i.e. $\beta \approx 2$), the CPU time was almost completely insensitive to h_{cutoff} in the range $0.5 \lesssim h_{cutoff} \lesssim 5$. We used $h_{cutoff} = 1.68474$ in our production runs.

Finally, let us make some remarks about the problem of generating a random vector $(\sigma^1, \dots, \sigma^{N-1})$ on the unit sphere of \mathbb{R}^{N-1} . For $N = 3$ this is easy: generate a uniform random angle $\theta \in [0, 2\pi]$ and take the cosine and sine. For $N = 4$ it is also easy: generate a uniform random variable $\sigma^1 \in [-1, 1]$, and then generate a random vector (σ^2, σ^3) on the circle of radius $[1 - (\sigma^1)^2]^{1/2}$ as just described. (This is the method we employed.) For $N > 4$ one can generate first σ^1 from a Beta $\left(\frac{N-2}{2}, \frac{N-2}{2}\right)$ distribution, then σ^2 from a Beta $\left(\frac{N-3}{2}, \frac{N-3}{2}\right)$ distribution scaled by $[1 - (\sigma^1)^2]^{1/2}$, and so forth. Numerous other methods are described in [82, Section V.4].

²⁰ In a Monte Carlo application, the h are themselves random variables, and the CPU time is proportional to $\langle A(h)^{-1} \rangle$ (not $\langle A(h) \rangle^{-1}$, as we once learned the hard way!). It is thus important to use a generator in which $A(h)$ stays away from zero, *even for “rare” values of h* . This is especially important in the MGMC application, in which an extremely wide range of values of h are observed on the different grids.

h	Acceptance Probability		
	Method 1	Method 2	Method 3
0.0000	0.7854	0.0000	1.0000
0.1000	0.7851	0.0359	0.9060
0.2000	0.7841	0.0922	0.8228
0.2521	0.7833	0.1243	0.7834
0.3000	0.7825	0.1543	0.7492
0.4000	0.7802	0.2168	0.6838
0.5000	0.7774	0.2772	0.6257
0.6000	0.7740	0.3343	0.5739
0.7000	0.7700	0.3873	0.5276
0.8000	0.7656	0.4361	0.4862
0.8603	0.7627	0.4634	0.4634
0.9000	0.7607	0.4806	0.4491
1.0000	0.7554	0.5212	0.4158
1.5000	0.7242	0.6724	0.2921
1.6847	0.7114	0.7114	0.2596
2.0000	0.6889	0.7631	0.2153
3.0000	0.6199	0.8545	0.1312
4.0000	0.5618	0.8961	0.0894
5.0000	0.5152	0.9191	0.0656
10.0000	0.3810	0.9612	0.0243
20.0000	0.2749	0.9809	0.0088
30.0000	0.2259	0.9874	0.0048
40.0000	0.1963	0.9906	0.0031
50.0000	0.1759	0.9925	0.0022
100.0000	0.1249	0.9962	0.0008
200.0000	0.0885	0.9981	0.0003
500.0000	0.0560	0.9992	0.0001
∞	0.0000	1.0000	0.0000

Table 8: Acceptance probability for generating a random variable from (A.3) with $N = 4$, using rejection from e^{ht} (method 1), rejection from gamma (method 2) or rejection from beta (method 3).

References

- [1] A.D. Sokal, *Monte Carlo Methods in Statistical Mechanics: Foundations and New Algorithms*, Cours de Troisième Cycle de la Physique en Suisse Romande (Lausanne, June 1989).
- [2] S.L. Adler, Nucl. Phys. B (Proc. Suppl.) **9**, 437 (1989).
- [3] U. Wolff, Nucl. Phys. B (Proc. Suppl.) **17**, 93 (1990).
- [4] A.D. Sokal, Nucl. Phys. B (Proc. Suppl.) **20**, 55 (1991).
- [5] J. Goodman and A.D. Sokal, Phys. Rev. Lett. **56**, 1015 (1986).
- [6] J. Goodman and A.D. Sokal, Phys. Rev. **D40**, 2035 (1989).
- [7] R.G. Edwards, J. Goodman and A.D. Sokal, Nucl. Phys. **B354**, 289 (1991).
- [8] A. Hulsebos, J. Smit and J.C. Vink, Nucl. Phys. **B356**, 775 (1991).
- [9] N.D. Mermin, J. Math. Phys. **8**, 1061 (1967).
- [10] O.A. McBryan and T. Spencer, Commun. Math. Phys. **53**, 299 (1977).
- [11] C.-E. Pfister, Commun. Math. Phys. **79**, 181 (1981).
- [12] J. Bricmont, J.-R. Fontaine and L.J. Landau, Commun. Math. Phys. **56**, 281 (1977).
- [13] A. Messenger, S. Miracle-Solé and C.-E. Pfister, Commun. Math. Phys. **58**, 19 (1978).
- [14] A.B. Zamolodchikov and A.B. Zamolodchikov, Nucl. Phys. **B133**, 525 (1978); Ann. Phys. (N.Y.) **120**, 253 (1979).
- [15] A. Polyakov and P.B. Wiegmann, Phys. Lett. **131B**, 121 (1983).
- [16] P.B. Wiegmann, Phys. Lett. **152B**, 209 (1985); Pis'ma Zh. Eksp. Teor. Fiz. **41**, 79 (1985) [= JETP Lett. **41**, 95 (1985)].
- [17] P. Hasenfratz, M. Maggiore and F. Niedermayer, Phys. Lett. **B245**, 522 (1990).
- [18] P. Hasenfratz and F. Niedermayer, Phys. Lett. **B245**, 529 (1990).
- [19] P. Hasenfratz and F. Niedermayer, Exact mass gap and the thermodynamic Bethe Ansatz for the $O(N)$ σ -model, Max-Planck-Institut preprint MPI-PAE/PTh 3/91 (January 1991).
- [20] A.M. Polyakov, Phys. Lett. **B59**, 79 (1975).
- [21] E. Brézin and J. Zinn-Justin, Phys. Rev. **B14**, 3110 (1976).
- [22] D.J. Amit and G.B. Kotliar, Nucl. Phys. **B170**[FS1], 187 (1980).
- [23] G. Parisi, Phys. Lett. **B92**, 133 (1980).

- [24] J. Shigemitsu and J.B. Kogut, Nucl. Phys. **B190**[FS3], 365 (1981).
- [25] W. Bernreuther and F.J. Wegner, Phys. Rev. Lett. **57**, 1383 (1986).
- [26] M. Falcioni and A. Treves, Nucl. Phys. **B265**, 671 (1986).
- [27] T. Jolicoeur and J.C. Niel, Nucl. Phys. **B300**[FS22], 517 (1988).
- [28] T. Jolicoeur and J.C. Niel, Phys. Lett. **B215**, 735 (1988).
- [29] P. Weisz and M. Lüscher, unpublished, cited in [46].
- [30] P. Butera, M. Comi and G. Marchesini, Nucl. Phys. **B300**[FS22], 1 (1988).
- [31] P. Butera, M. Comi, G. Marchesini and E. Onofri, Nucl. Phys. **B326**, 758 (1989).
- [32] P. Butera, M. Comi and G. Marchesini, Phys. Rev. **B41**, 11494 (1990).
- [33] V.F. Müller, T. Raddatz and W. Rühl, Nucl. Phys. **B251**[FS13], 212 (1985); erratum, Nucl. Phys. **B259**, 745 (1985).
- [34] H. Flyvbjerg, Phys. Lett. **B219**, 323 (1989).
- [35] J.-M. Drouffe and H. Flyvbjerg, Nucl. Phys. **B332**, 687 (1990).
- [36] H. Flyvbjerg and S. Varsted, Nucl. Phys. **B344**, 646 (1990); H. Flyvbjerg and F. Larsen, Phys. Lett. **B266**, 92, 99 (1991).
- [37] H. Flyvbjerg, Phys. Lett. **B245**, 533 (1990).
- [38] P. Biscari, M. Campostrini and P. Rossi, Phys. Lett. **B242**, 225 (1990); M. Campostrini and P. Rossi, Phys. Lett. **B242**, 81 (1990).
- [39] U.M. Heller, Phys. Rev. Lett. **60**, 2235 (1988).
- [40] U.M. Heller, Phys. Rev. **D38**, 3834 (1988).
- [41] U. Wolff, Phys. Rev. Lett. **62**, 361 (1989).
- [42] R.G. Edwards and A.D. Sokal, Phys. Rev. **D40**, 1374 (1989).
- [43] M. Hasenbusch, Nucl. Phys. **B333**, 581 (1990).
- [44] U. Wolff, Nucl. Phys. **B334**, 581 (1990).
- [45] P. Hasenfratz and F. Niedermayer, Nucl. Phys. **B337**, 233 (1990).
- [46] U. Wolff, Phys. Lett. **B248**, 335 (1990); Nucl. Phys. B (Proc. Suppl.) **20**, 682 (1991).
- [47] M. Hasenbusch, S. Meyer and G. Mack, Nucl. Phys. B (Proc. Suppl.) **20**, 110 (1991).
- [48] J. Apostolakis, C.F. Baillie and G.C. Fox, Phys. Rev. **D43**, 2687 (1991).

- [49] S. Caracciolo, R.G. Edwards, A. Pelissetto and A.D. Sokal, Wolff-type embedding algorithms for general nonlinear σ -models, in preparation. A preliminary version of this work has appeared in Nucl. Phys. B (Proc. Suppl.) **20**, 72 (1991).
- [50] K.R. Ito, Phys. Rev. Lett. **58**, 439 (1987).
- [51] K.R. Ito, Prog. Theor. Phys. Suppl. **92**, 46 (1987).
- [52] K.R. Ito, Phys. Rev. Lett. **64**, 2839 (1990).
- [53] K.R. Ito, Commun. Math. Phys. **139**, 45 (1991).
- [54] A. Patrascioiu, Phys. Rev. Lett. **58**, 2285 (1987).
- [55] E. Seiler, I.O. Stamatescu, A. Patrascioiu and V. Linke, Nucl. Phys. **B305**[FS23], 623 (1988).
- [56] A. Patrascioiu, E. Seiler and I.O. Stamatescu, Nuovo Cim. **11D**, 1165 (1989).
- [57] H. Meyer-Ortmanns, Z. Phys. **C27**, 553 (1985).
- [58] W. Hackbusch, *Multi-Grid Methods and Applications* (Springer, Berlin, 1985).
- [59] G. Mack, Nucl. Phys. **B235**, 197 (1984).
- [60] S.F. McCormick and J. Ruge, Math. Comput. **41**, 43 (1983).
- [61] K. Fredenhagen and M. Marcu, Phys. Lett. **B193**, 486 (1987).
- [62] J. Mandel, S. McCormick and R. Bank, in *Multigrid Methods*, ed. S.F. McCormick (SIAM, Philadelphia, 1987), Chapter 5.
- [63] J. Goodman and A.D. Sokal, unpublished.
- [64] A. Brandt, Appl. Math. Comput. **19**, 23 (1986).
- [65] A.D. Sokal, unpublished.
- [66] J. Linn, Diploma Thesis, University of Kaiserslautern (1991), cited in [47].
- [67] G. Mack, in *Nonperturbative Quantum Field Theory* (1987 Cargèse lectures), ed. G. 't Hooft *et al.* (Plenum, New York, 1988).
- [68] G. Mack and S. Meyer, Nucl. Phys. B (Proc. Suppl.) **17**, 293 (1990).
- [69] M. Hasenbusch and S. Meyer, Multigrid acceleration for asymptotically free theories, Kaiserslautern preprint Th 91-16 (September 1991).
- [70] M.B. Priestley, *Spectral Analysis and Time Series*, 2 vols. (Academic, London, 1981).
- [71] T.W. Anderson, *The Statistical Analysis of Time Series* (Wiley, New York, 1971).
- [72] N. Madras and A.D. Sokal, J. Stat. Phys. **50**, 109 (1988).

- [73] S. Caracciolo, A. Pelissetto and A.D. Sokal, *J. Stat. Phys.* **60**, 1 (1990).
- [74] G. Parisi, in *Progress in Gauge Field Theory* (1983 Cargèse lectures), ed. G. 't Hooft *et al.* (Plenum, New York, 1984).
- [75] G.G. Batrouni, G.R. Katz, A.S. Kronfeld, G.P. Lepage, B. Svetitsky and K.G. Wilson, *Phys. Rev.* **D32**, 2736 (1985).
- [76] E. Dagotto and J.B. Kogut, *Phys. Rev. Lett.* **58**, 299 (1987).
- [77] E. Dagotto and J.B. Kogut, *Nucl. Phys.* **B290**[FS20], 451 (1987).
- [78] P.J. Rossky, J.D. Doll and H.L. Friedman, *J. Chem. Phys.* **69**, 4628 (1978); R.T. Scalettar, D.J. Scalapino and R.L. Sugar, *Phys. Rev.* **B34**, 7911 (1986); M. Creutz, *Phys. Rev.* **D38**, 1228 (1988).
- [79] S. Duane, A.D. Kennedy, B.J. Pendleton and D. Roweth, *Phys. Lett.* **B195**, 216 (1987); M. Creutz, *Phys. Rev.* **D38**, 1228 (1988); H. Gausterer and S. Sanielevici, *Phys. Rev.* **D38**, 1220 (1988); R. Gupta, G.W. Kilcup and S.R. Sharpe, *Phys. Rev.* **D38**, 1278 (1988); A.D. Kennedy, *Nucl. Phys. B (Proc. Suppl.)* **9**, 457 (1989).
- [80] R.H. Swendsen and J.-S. Wang, *Phys. Rev. Lett.* **58**, 86 (1987).
- [81] D.J. Best and N.I. Fisher, *Appl. Statist.* [= *J. Roy. Statist. Soc., Series C*] **28**, 152 (1979).
- [82] L. Devroye, *Non-Uniform Random Variate Generation* (Springer, New York, 1986).
- [83] D.E. Knuth, *The Art of Computer Programming*, vol. 2, 2nd ed. (Addison-Wesley, Reading MA, 1981), Section 3.4.1, pp. 120-121.
- [84] M. Creutz, *Phys. Rev.* **D21**, 2308 (1980).
- [85] K. Fabricius and O. Haan, *Phys. Lett.* **B143**, 459 (1984).
- [86] A.D. Kennedy and B.J. Pendleton, *Phys. Lett.* **B156**, 393 (1985).
- [87] P. de Forcrand, *J. Stat. Phys.* **43**, 1077 (1986).